A syngeneic spontaneous zebrafish model of *tp53*-deficient, EGFR^{vIII}, and PI3KCA^{H1047R}-driven glioblastoma reveals inhibitory roles for inflammation during tumor initiation and relapse *in vivo*

Alex Weiss[1], Cassandra D'Amata[1], Bret J. Pearson[2,3,4*], Madeline N. Hayes[1,2*]

[1]Developmental and Stem Cell Biology Program, The Hospital for Sick Children, Toronto, Canada
[2]Department of Molecular Genetics, University of Toronto, Toronto, Canada
[3] Knight Cancer Institute, Oregon Health & Science University, Portland, Oregon, 97239, USA
[4] Department of Pediatrics, Papé Research Institute, Oregon Health & Science University, Portland, Oregon, 97239, USA

*Correspondence:

Madeline N. Hayes
The Hospital for Sick Children PGCRL Building
686 Bay Street, Toronto, Ontario
M5G 0A4, Canada
Phone: 416-813-7654, ext. 328370
E-mail: madeline.hayes@sickkids.ca

Bret J. Pearson
3181 SW Sam Jackson Park Rd.
LBRB Room 305, L481
Portland, OR, 97239, USA
503-494-7979
E-mail: pearsobr@ohsu.edu

Keywords: Glioblastoma, Zebrafish, Oncogenesis, Tumor microenvironment

Disclosure of Potential Conflicts of Interest:
The authors declare no potential conflicts of interest.

Abstract

High-throughput vertebrate animal model systems for the study of patient-specific biology and new therapeutic approaches for aggressive brain tumors are currently lacking, and new approaches are urgently needed. Therefore, to build a patient-relevant *in vivo* model of human glioblastoma, we expressed common oncogenic variants including activated human EGFR^{vIII} and PI3KCA^{H1047R} under the control of the radial glial-specific promoter *her4.1* in syngeneic *tp53* loss-of-function mutant zebrafish. Robust tumor formation was observed prior to 45 days of life, and tumors had a gene expression signature similar to human glioblastoma of the mesenchymal subtype, with a strong inflammatory component. Within early stage tumor lesions, and in an *in vivo* and endogenous tumor microenvironment, we visualized infiltration of phagocytic cells, as well as internalization of tumor cells by *mpeg1.1*:EGFP+ microglia/macrophages, suggesting negative regulatory pressure by pro-inflammatory cell types on tumor growth at early stages of glioblastoma initiation. Furthermore, CRISPR/Cas9-mediated gene targeting of master inflammatory transcription factors *irf7* or *irf8* led to increased tumor formation in the primary context, while suppression of phagocyte activity led to enhanced tumor cell engraftment following transplantation into otherwise immune-competent zebrafish hosts. Altogether, we developed a genetically relevant model of aggressive human glioblastoma and harnessed the unique advantages of zebrafish including live imaging, high-throughput genetic and chemical manipulations to highlight important tumor suppressive roles for the innate immune system on glioblastoma initiation, with important future opportunities for therapeutic discovery and optimizations.

Introduction

Creating faithful models and discovering tailored treatments for patients with aggressive brain tumors has resulted in many different experimental platforms, each with their own unique advantages (Gómez-Oliva et al., 2021; Haddad et al., 2021). However, tractable vertebrate animal model systems for high-throughput study of tumor development in an intact and endogenous tumor microenvironment (TME) remain limited. New approaches that reflect patient genetics and physiology have the potential to aid in improving therapeutic strategies for individuals with malignant brain tumors like glioblastoma, which represents about 50% of all primary brain malignancies in adults (Ostrom et al., 2017; Torp et al., 2022).

Despite intensive treatments including surgery, radiation, and chemotherapy (temozolomide, TMZ), most patients with glioblastoma eventually relapse and have a median survival rate of less than 15 months (Aldape et al., 2019). Therapeutic resistance can partly be attributed to a poor understanding of underlying molecular mechanisms, as well as a significant level of heterogeneity between patients and within individual tumors. Molecular heterogeneity has been important for the classification of three major subtypes of glioblastoma including proneural, classical, and mesenchymal (Brennan et al., 2013; Torp et al., 2022; Verhaak et al., 2010; Wang et al., 2017). However, recent evidence supporting co-existence of inter-converting glioblastoma cell states within individual patient tumors reveals less distinct subtype separations and phenotypic flexibilities that contribute to the aggressiveness and drug resistance of glioblastoma across molecular cohorts (Darmanis et al., 2017; Neftel et al., 2019; Patel et al., 2014).

In general, 90% of glioblastoma tumors display alterations in core signaling factors involved in Receptor Tyrosine Kinase (RTK)/RAS/PI3K pathway activation (Brennan et al., 2013; McLendon et al., 2008). While activating mutations in RAS proteins are rarely found in the clinic, loss of the negative regulator *NF1* is common, as well as amplifications and/or activating mutations in various RAS pathway activators including Epidermal Growth Factors Receptor (EGFR), which are found in >50% of glioblastomas (Brennan et al., 2013; Hoogstrate et al., 2022; McLendon et al., 2008). Loss of the lipid phosphatase PTEN and/or activating mutations in the PI3K catalytic subunit PIK3CA are also commonly found, which altogether drive downstream activation of oncogenic RAS/MAPK and AKT/mTOR signaling, among other crucial pathways involved in growth and survival of glioblastoma (Brennan et al., 2013; McLendon et al., 2008). Furthermore, the TP53 tumor suppressor pathway is altered in 84% of globlastoma patients and 94% of cell lines, with TP53 loss implicated in proliferation, invasion, migration, and stemness (Brennan et al., 2013; McLendon et al., 2008; Zhang et al., 2018). Importantly, single pathway mutations are generally insufficient to transform normal brain tissues, and multiple mutations are required for glioma formation (Chen et al., 2018; Haddad et al., 2021; Holland et al., 2013; Takke et al., 1999). Therefore, to recapitulate human glioblastoma in experimental models, multiple genetic events should be considered.

In addition to key genetic drivers, the TME is known to influence cellular flexibility in glioblastoma and consists of heterogeneous collections of resident brain, stroma, and immune cells, as well as cells recruited from the general circulation such as bone marrow-derived immune cells with known tumor suppressive and tumor promoting functions (Bikfalvi et al., 2023; Quail and Joyce, 2017). Given emerging opportunities for harnessing the immune system for the treatment of human cancer, there is a growing focus on understanding innate and

adaptive immune responses across different subtypes of human malignancies. However, like many other tumors, glioblastoma combines a lack of immunogenicity due to few mutations with a highly immunosuppressive tumor microenvironment. In addition to off-target effects of current frontline therapeutic strategies, both tumor and immune cells contribute to immune suppression in and surrounding the TME in glioblastoma (McGranahan et al., 2019; Sengupta et al., 2012), which could explain the failure of immunotherapy-based clinical trials. Additionally, lymphocytes are frequently exhausted and dysfunctional and therefore inadequate at exerting an anti-tumor immune response, while tumor-associated myeloid cells are frequently reprogrammed by signaling from tumor cells and the TME to cell states that promote glioblastoma survival, growth, and invasion (Kennedy et al., 2013; McGranahan et al., 2019; Pearson et al., 2020). Evidence also supports tumor-cell intrinsic mechanisms in response to immune cell attack leading to various evasion mechanisms, including upregulation of myeloid-associated gene expression programs and resistance to interferon signaling (Gangoso et al., 2021; Parmigiani et al., 2022).

Complex intercellular communication in glioblastoma highlights the importance of faithful *in vivo* models. However, roles for the endogenous TME especially at early stages of tumor initiation, remain poorly understood. Furthermore, live visualization of heterogeneity and tumor cells within the TME is limited in non-transparent rodent genetic models and/or patient-derived tumor xenografted hosts. Therefore, here our goal was to develop a patient-relevant model of aggressive human glioma in an intact and immune competent system. We developed a novel spontaneous, syngeneic zebrafish model of glioblastoma, with high levels of inflammatory immune cell infiltration and anti-tumor associations between phagocytes in the TME and tumor cells, suggesting inhibitory roles for inter-cellular interactions during glioblastoma initiation and an effective *in vivo* platform for future biological discovery and drug testing for patients.

Results

Oncogenic MAPK/AKT pathway activation drives glial-derived tumor formation in syngeneic *tp53* mutant zebrafish

To generate a patient-relevant brain tumor model in zebrafish we used the zebrafish *her4.1* promoter to simultaneously over-express constitutively active human EGFR ($EGFR^{vIII}$) and PI3KCA ($PI3KCA^{H1047R}$) variants in neural progenitors and radial glia of syngeneic *tp53* loss-of-function mutant larvae (Ignatius et al., 2018; Takke et al., 1999; Than-Trong et al., 2020). Co-injection of linearized *her4.1*:**E**GFR^{vIII} + *her4.1*:**P**$I3KCA^{H1047R}$ + *her4.1*:m**S**carlet transgenes into syngeneic (CG1) *tp53*$^{-/-}$ mutant embryos at the one-cell stage led to broad transient mScarlet expression for 5-6 days followed by rare mosaic expression in the anterior CNS (henceforth referred to as p53EPS, Fig 1A), as expected from a transient mosaic injection strategy used to express stable concatemers of DNA vectors (Langenau et al., 2008). At 15 days post fertilization (dpf), this transgene combination led to visible mScarlet-positive brain lesions in the anterior CNS of live zebrafish (Fig 1B-D). Injections of single linearized vector and vector combinations resulted in a maximum incidence of approximately 15-20% affected zebrafish induced by the p53EPS combination by 45 dpf (Fig 1D). Inter-tumoral variability was observed among p53EPS mosaic-injected zebrafish, with tumors of variable size arising in different brain regions including the telencephalon and diencephalon regions (8/29 = 27.5%, from three independent tumor screens), and the optic tectum/mesencephalon region (21/29 = 72.5%, from three independent tumor screens) (Supplementary Fig 1). To further define the tissue of origin of zebrafish p53EPS CNS lesions, we co-injected linearized *gfap*:EGFP (Don et al., 2017) and

visualized EGFP expression in 100% of brain masses at 30-40 dpf (Fig 1A,B), supporting glial identity and a novel *in vivo* model of malignant glioma.

To test for transformation of p53EPS cells from primary mosaic-injected animals, we harvested bulk tissue from dissected zebrafish brains and transplanted dissociated cells into the hindbrain ventricles of 2 dpf syngeneic *tp53* wild-type (CG1) zebrafish (Mizgireuv and Revskoy, 2006). At approximately 18 days post-transplant (18 dpt, or 20 dpf), we screened for mScarlet+ fluorescence and visualized her4.1+/gfap+ tumor cell outgrowth in 16-25% of transplanted hosts (n=3 independent screens, Fig 1E,F), supporting oncogenic transformation and malignant growth *in vivo* of p53EPS cells. Fluorescence activated cell sorting (FACS) revealed fluorescently labeled tumor cells in un-labeled syngeneic host brains and co-expression of *her4.1*:mScarlet/*gfap*:EGFP (Fig 1G), further supporting tumor growth from a glial-derived progenitor cell, which was expected from *her4.1*-specific oncogene activation during zebrafish development (Than-Trong et al., 2020).

We performed serial sectioning of uninjected control and primary p53EPS zebrafish brains and performed histological characterizations, which revealed highly aggressive and proliferative tumors in p53EPS consisting of a heterogenous mix of different malignant cell types, compared to normal brains (Fig 1H-O, Supplementary Fig 2). One major cell type displayed a round granular-like morphology with a high nuclear to cytoplasm ratio, while a second cell type found within the same tumor masses displayed a flattened and elongated morphology (Fig 1L, Supplementary Fig 2). In general, tumors displayed clean margins without invasive boundaries, necrosis, or micro vascularization; however, a few instances of cell migration along vasculature were detected. Certain p53EPS tumors displayed embryonal features including rosette-type

structures and a high mitotic index, overlapping histological features with glioblastoma with primitive neuronal component (Suwala et al., 2021), which may be expected given our chosen combination of molecular drivers as well as a neural progenitor and/or radial glial cell of origin, during developmental stages.

To assess oncogenic signaling pathway activation, we stained unaffected and p53EPS tumor-positive brain sections for phosphorylated-ERK (p-ERK) and phosphorylated-AKT (p-AKT), indicators of activated MAPK and AKT signaling pathways, respectively (Fig 1J-K, N-O). Compared to normal brains, we found increased p-ERK and p-AKT staining within tumor lesions, consistent with elevated MAPK and AKT activation driving malignant transformation (Fig 1N-O). To further validate effects of relevant downstream signaling pathway activation, we also co-injected linearized *her4.1*:**K**RAS^{G12D} + *her4.1*:**P**I3KCA^{H1047R} + *her4.1*:m**S**carlet into *tp53*$^{-/-}$ embryos (p53KPS). At 15-20 dpf, we visualized tumor onset and penetrance comparable to p53EPS (Supplementary Fig 3), suggesting a dominant role for MAPK/AKT pathway activation downstream of RTK signaling in driving tumor formation, and a flexible oncogenic strategy for inducing robust brain tumor formation in zebrafish.

Gene set enrichment analyses (GSEA) reveal gene expression patterns consistent with human mesenchymal glioblastoma and inflammation.

To further characterize our novel zebrafish brain tumor models, we performed bulk RNA sequencing (RNAseq) of three independent p53EPS tumor-burdened brains, three independent p53KPS tumor-burdened brains, and three age-matched, control-injected zebrafish brains that remained tumor-free at the time of harvesting tissue. Using hierarchical clustering on normalized

gene expression, our tumor-free control samples clustered together and apart from p53EPS and p53KPS tumor brains, which displayed a recognizable level of transcriptional variability across principal components (Fig 2A). Interestingly, p53EPS and p53KPS samples failed to cluster according to oncogenic drivers (Fig 2A), suggesting molecular similarities as well as inter-tumor heterogeneity reflecting differences in tumor location, size, and contribution of tumor cells to total sample inputs.

Given the relevance of our p53EPS driver combination to human glioblastoma, we chose to focus the remainder of our molecular analyses on p53EPS samples. Using differential gene expression analysis, we identified a conserved set of differentially expressed (DE) genes in p53EPS tumor brains, with 236 significantly upregulated and 28 downregulated genes, compared to control injected brains at 20-30 dpf ($2 > \text{log2foldChange} > -2$, adjusted p-value < 0.05, Supplementary Table 1, Supplementary Table 2, Fig 2B). Using human orthologs of differentially expressed genes, we performed Gene Set Enrichment Analysis (GSEA) (Mootha et al., 2003; Subramanian et al., 2005), comparing our p53EPS zebrafish model to published expression patterns for human glioblastoma subtypes, as well as embryonal brain tumors including designated subtypes of medulloblastoma (Cavalli et al., 2017; McLendon et al., 2008; Wang et al., 2017). Among these gene sets, we found a significant enrichment for the mesenchymal subtype of human glioblastoma in p53EPS differentially expressed genes (Fig 2C, Supplementary Table 3) (McLendon et al., 2008; Wang et al., 2017). In contrast, while certain genes for other glioblastoma and/or medulloblastoma subtypes were upregulated in p53EPS samples, no significant enrichment was found for these specific gene expression signatures (Supplementary Fig 4, Supplementary Table 3) (Cavalli et al., 2017; McLendon et al., 2008; Wang et al., 2017).

To assess potential underlying molecular mechanisms involved in p53EPS formation, we assessed enrichment for Hallmark gene expression sets available through the Molecular Signature Database (MSigDB, Supplementary Table 4) (Liberzon et al., 2011). Interestingly, 7 of the top 13 enriched gene sets identified (NOM p-value <0.05) related to inflammation or inflammatory signaling pathways, including the Interferon gamma response, TNFA signaling, the Interferon alpha response, and Jak/STAT3 signaling (Fig 2D, Supplementary Table 4), suggesting a strong inflammatory component in our brain tumor model. Additional pathway signatures included those related to RAS signaling, Hypoxia, and Epithelial-to-Mesenchymal Transitions (EMT) (Supplementary Table 4), suggesting on target oncogenic pathway activation, hypoxia, and invasive properties, consistent with aggressive glioblastoma (Majc et al., 2020; Park and Lee, 2022). Therefore, bulk RNA sequencing expression data supports significant molecular similarity between our zebrafish p53EPS brain tumor model and human glioblastoma of the mesenchymal subtype, with a significant inflammatory component.

Given the *in vivo* context and contribution of tumor and non-tumor cell types to our bulk RNAseq analysis, we decided to assess RNA expression in FACS-sorted *her4.1:*mScarlet-positive tumor cells, as well as *her4.1*:mScarlet-negative bulk stromal cells, compared to non-tumor whole brain tissue (Fig 2E, Supplementary Table 5). Interestingly, we observed increased immune cell and inflammatory gene expression in both p53EPS tumor and stromal cell fractions compared to control unaffected whole brain tissue, including transcripts associated with myeloid cell types (*mpeg1, irf7, irf8*), lymphoid progenitor and specific subtype regulators (*rag1, rag2, lck*), *stat1a/b*, *fas* cell surface death receptor, and toll-like receptor 4b (*tlr4bb*), among others genes involved in immune responses (adjusted p-value < 0.0001, Fig 2E, Supplementary Table 5). We

validated a selection of genes from RNAseq using RT-PCR (Supplementary Fig 5), as well as transient co-injection of linearized transgene with our EPS mix to assess tumor cell-specific expression of lymphoid *rag2*:EGFP and myeloid *mpeg1.1:*EGFP at 30 dpf (Fig 2F-I). Interestingly, we observed co-expression of *her4.1*:mScarlet/*rag2*:EGFP and *her4.1*:mScarlet/*mpeg1.1*:EGFP in p53EPS tumors (Fig 2F-I), suggesting promoter activity at certain immune-associated genes within established p53EPS tumor cells *in vivo.* These data suggest inflammation-associated gene expression in both zebrafish glioblastoma-like cells and the TME and is consistent with inflammatory gene expression in tumor cells associated with immune evasion and *in vivo* growth in other models (Gangoso et al., 2021; Yang et al., 2022). Altogether, our *in vivo* expression data supports p53EPS zebrafish as a comparable and relevant model system to study glioblastoma tumor biology, as well as intercellular interactions within an endogenous TME.

Zebrafish mesenchymal glioblastoma-like tumors recruit activated mononuclear phagocytes at early stages of tumor formation

Given that p53EPS tumor-burdened brains displayed strong enrichment for transcriptional signatures associated with inflammatory signaling, we were interested in the role for innate immune cells in the earliest stages of p53EPS tumor formation. Myeloid cells including microglia and macrophages are recruited in many different subtypes of primary brain tumors and in brain metastases (Gutmann and Kettenmann, 2019; Khan et al., 2023). However, how phagocyte populations affect glioblastoma initiation is less well understood given that most studies utilize established tumor cell models and/or patient derived tissue xenograft transplantations into immune-compromised host animals. To first determine whether myeloid-derived phagocytic cell

lineages are enriched in p53EPS lesions at early stages of tumor initiation, we used neutral red staining that labels lysosomal-rich phagocytes, irrespective of cell type (Fig 3A-C) (Herbomel et al., 2001a; Shiau et al., 2015). At 10 dpf, we observed enrichment of neutral red-positive foci in regions of *her4.1*:mScarlet+ fluorescent intensity (Fig 3B,C), suggesting phagocyte infiltration during p53EPS initiation, prior to typical observation of macroscopic tumor masses (Fig 1D). To assess the activation state of phagocytes in and surrounding p53EPS tumors, we co-injected our oncogene combination into *tp53*$^{-/-}$ embryos carrying a Tg(*tnfa*:EGFP) transgenic marker of activated and pro-inflammatory phagocytes (Hao et al., 2012; Nguyen-Chi et al., 2015), and observed enrichment of *tnfa*:EGFP single-positive cells in *her4.1*:mScarlet+ lesions (Fig 3D,E). We also performed GSEA against immunologic signature gene sets from the Molecular Signatures Database (MSigDB, (Liberzon et al., 2011; Mootha et al., 2003; Subramanian et al., 2005)), and identified multiple enriched gene expression signatures associated with inflammation and inflammatory cell types in p53EPS tumor-burdened brains (Supplementary Table 6). p53EPS displayed features of both pro- and anti-inflammatory gene expression, which is consistent with a mixed immune activation/suppressive state in glioblastoma known to play an important role in tumor progression in patients (Biswas et al., 2008; Karimi et al., 2023; Quail and Joyce, 2017; Ren et al., 2023). However, p53EPS tissues more significantly enriched for gene expression associated with activated and pro-inflammatory phagocytes including classical M1 macrophages, compared to alternative M2 polarized macrophages, and genes typically downregulated during M2 polarization following macrophage colony stimulating factor (M-CSF) treatment (Supplementary Fig 6, Supplementary Table 6), further suggesting strong promotion of inflammation within the TME.

Given enrichment for *tnfa*:EGFP+ phagocytes and signatures associated with pro-inflammatory macrophages in our glioblastoma model, we decided to investigate microglia/macrophages cell dynamics *in vivo* using live confocal imaging following co-injection of the linearized transgene combination into *tp53*$^{-/-}$; Tg(*mpeg1.1*:EGFP) zebrafish (Ellett et al., 2011). We first looked closely at a time-course of lesion formation at 5, 7, and 9 dpf relative to microglia in the zebrafish brain (Fig 3F-K), which colonize the zebrafish neural retina by 48 hpf, and the optic tectum by 84 hpf (Herbomel et al., 2001). At 5 dpf (120 hpf), we observed comparable levels of *mpeg1.1:*EGFP+ microglia throughout the cephalic region and in the brain in both control and p53EPS injected zebrafish (Fig 3F,I). p53EPS-injected zebrafish brains displayed mosaic cellular expression of *her4.1*:mScarlet; however, cells were sparse and diffuse, and no large intensely fluorescent tumor-like clusters were detected at this stage (Fig 3I, n=12/12 tumor negative). At 7 dpf, we detected small clusters of *her4.1*:mScarlet+ cells (Fig 3J, n=5/9), indicative of early lesion formation. Interestingly, these lesions were surrounded and/or infiltrated by *mpeg1.1:*EGFP+ microglia, while at 9 dpf *her4.1*:mScarlet+ expression became highly specific to tumor lesions, and these lesions were consistently associated with *mpeg1.1:*EGFP+ microglia/macrophages (Fig 3K, n=8/8 tumor-positive zebrafish).

At 12 dpf in p53EPS zebrafish with established tumors, we observed fluorescent *mpeg1.1:*EGFP+ cells surrounding and within regions of concentrated *her4.1*:mScarlet+ fluorescence (Fig 3L, Movie 1). Microglia/macrophages outside of early-stage *her4.1:*mScarlet+ lesions displayed highly ramified morphologies, with several processes that were extended and retracted, indicative of environmental surveillance (Fig 3L, Movie 1) (Nimmerjahn A et al., 2005). *mpeg1.1:*EGFP+ microglia/macrophages infiltrated into dense *her4.1:*mScarlet+ regions displayed more rounded and amoeboid-like morphology, supporting their activation in

association with p53EPS oncogenic cells (Karperien et al., 2013). Interestingly, *mpeg1.1:*EGFP+ microglia/macrophages dynamically interacted with *her4.1*:mScarlet+ cells (Movies 1 and 2), and in p53EPS oncogenic masses, *mpeg1.1:*EGFP+ microglia/macrophages associated closely with and often displayed internalized *her4.1:*mScarlet+ punctate cells (Fig 3L,M), suggesting engulfment and removal of p53EPS cells during tumor formation *in vivo*. Together with our expression data, visualization of infiltrating myeloid-derived immune cells in p53EPS glioblastoma-like lesions, dynamic *mpeg*+ microglia/macrophages-p53EPS interactions, and tumor cell engulfment suggests anti-tumoral activity at early stages that could negatively affect tumor formation *in vivo*.

Inflammation-associated *irf7* and *irf8* are required to inhibit p53EPS tumor formation *in vivo*

Interferon regulatory factor (Irf) proteins regulate transcription of interferon genes and support a variety of different immune reposes. Irf7 and Irf8 are critical for global activation of the type I IFN response following stimulation and for myeloid cell development, respectively (Günthner and Anders, 2013; Ning et al., 2011; Shiau et al., 2015). Irf8 is a conserved determinant of macrophage cell fate, as well as dendritic cell survival and function, and *irf8* mutant zebrafish lack microglia/macrophages in the brain up to 31 dpf (Shiau et al., 2015; Sichien et al., 2016). Irf7 also drives differentiation of macrophages; however, in zebrafish and other systems, Irf7 is more broadly activated in immune cells in response to infection, with evidence also supporting non-immune cell-related functions during development and cancer progression (Feng et al., 2016; Gangoso et al., 2021; Günthner and Anders, 2013; Hu et al., 2022; Ning et al., 2011; Yang et al., 2022). Interestingly, we observed upregulation of several interferon regulatory factor

(Irf) family members including *irf7* and *irf8* in p53EPS tumor-burdened brains (Fig 2B, Supplementary Table 1, 2), suggesting potential roles for these master regulators of inflammation on immune-related responses during p53EPS tumorigenesis *in vivo*. Therefore, to assess functional roles for Irf7 and Irf8 in p53EPS formation, we used a transient CRISPR/Cas9 gene targeting approach to knock-down *irf7* or *irf8* genes prior to p53EPS tumor formation using co-injection of 2-3 gRNAs each targeting *irf7* or *irf8* (Supplementary Table 7), together with Cas9 protein and linearized EPS into one-cell stage *tp53*$^{-/-}$ embryos. At 2-5 dpf, we extracted DNA from a subset of injected embryos and observed a gene targeting efficiency of >90% and >65% INDELS at the *irf7* or *irf8* loci, respectively (ICE analysis, ice.synthego.com, Synthego, 2019). Gene transcript knock-down was also verified using RT-PCR (Supplementary Fig 7). Consistent with previous reports, *irf8* knock-down resulted in significant reductions in neutral red-positive phagocytes at 8-10 dpf (Supplementary Fig 8) (Shiau et al., 2015), and while no significant differences in neutral red-positive phagocyte number were observed following *irf7* gene targeting, *irf7* CRISPR/Cas9-injected animals displayed early mortality un-related to brain tumor formation, with ~80% of CRISPR-injected animals displaying illness prior to two months of age, consistent with a broad requirement for Irf7 in immune responses, among other functions.

Remarkably, following *irf7* or *irf8* gene knock-down with p53EPS, we observed robust tumor formation, with 65% of *irf7*-targeted and 42% of *irf8*-targeted p53EPS zebrafish developing tumors by 30 dpf, compared to 20% p53EPS incidence (Fig 4A-D, *irf7* $p<0.0001$, *irf8* $p=0.0155$, Fisher's exact test), suggesting an important inhibitory role for *irf7* and *irf8* in p53EPS tumor initiation. In p53EPS tumor brains with *irf7* and *irf8* knock-down, we observed reduced expression of genes associated with our inflammation signature in p53EPS tumor-burdened

brains, including immune evasion-associated transcripts like *suppressor of cytokine signaling 1a* (*socs1a*) (Supplementary Fig 7), suggesting reduced tumor-specific inflammation and associated immune-evasion mechanisms, which were previously shown to be upregulated in response to anti-tumor cell infiltration (Gangoso et al., 2021). To further validate gene targeting and assess the spatial localization of *irf7* expression within the TME, we performed fluorescent *in situ* hybridization (FISH) in control and *irf7* knock-down tumors and detected robust transcript expression within early-stage p53EPS lesions at 8 dpf (Fig 4E). In animals co-injected with *irf7* CRISPR, we detected p53EPS tumor formation, albeit with reduced *irf7* in and surrounding tumor cells (Fig 4E), suggesting potential roles for *irf7* in inhibiting p53EPS initiation in tumor cells and/or within the TME.

Given broad Irf gene expression in p53EPS tumors (Fig 2E, Supplementary Fig 5, 7, 9, Supplementary Table 5), as well as reports of *IRF7* gene expression in human glioblastoma tumor cells, association with worsened patient outcome, and potential roles in tumor stem cell biology (Jin et al., 2012; Yang et al., 2022), we decided to investigate tumor cell-specific roles for Irf genes in p53EPS initiation. To specifically knock-down *irf7* in p53EPS tumor cells, we generated a transgenic Tg(*her4.1*:Cas9-2A-EGFP);*tp53*$^{-/-}$ zebrafish strain and co-injected embryos with linearized EPS + gRNAs targeting *irf7* (Fig 4F). Despite a gene targeting efficiency of ~28% in pooled tumor cells from 5 tumor-burdened animals, we did not observe any significant changes in p53EPS tumor formation in Cas9-2A-EGFP-positive zebrafish compared to Cas9-2A-EGFP-negative control injected siblings (Fig 4F-H). We observed similar effects following co-injection of gRNAs targeting *irf8* (Fig 4G), suggesting that increased p53EPS tumor initiation following *Irf* gene knock-down is a consequence of *irf7* and *irf8* loss-of-function in the TME.

Phagocyte activity suppresses p53EPS engraftment following transplant into syngeneic host zebrafish

Given conserved roles for *irf8* across species in the specification and function of different phagocyte populations (Shiau et al., 2015), our functional data suggested an anti-tumor role for *irf/*phagocyte activity in the TME during p53EPS tumor initiation. To assess the role more specifically for phagocyte populations within the TME, we decided to transplant p53EPS tumor cells into the hindbrain ventricle of syngeneic host embryos at 2 dpf. Importantly, serial transplantation of tumor cells is commonly used as an experimental surrogate to assess relapse potential (Blackburn et al., 2011; Hayes et al., 2018; Ignatius et al., 2017; Smith et al., 2010), allowing us to use p53EPS engraftment and re-growth to study the tumor propagating properties of p53EPS within different TMEs. To test the role for phagocytes in engraftment, we transplanted dissociated bulk tumor cells into syngeneic embryos along with Clodronate (Clodronate liposomes, Clodrosomes), a chemical used to eliminate phagocytes *in vivo*, and microglia following intracerebral injection (Andreou et al., 2017; Fernández-López et al., 2016; Hanlon et al., 2019; Yan et al., 2019; Yang et al., 2021). At 18 days post-transplant (20 dpf), we observed 50% p53EPS tumor cell engraftment in host animals co-injected with Clodronate, compared to 23% injected with vehicle control liposomes (p=0.0048, Fisher's exact test, Fig 5A-C). Interestingly, while p53EPS engrafted brains maintained inflammatory gene expression patterns like primary p53EPS tumor-burdened brains (Supplementary Fig 9A), co-transplantation with Clodronate inhibited inflammatory gene expression in bulk tissue (Supplementary Fig 9B, normalized to mScarlet expression to control for differences in tumor size), suggesting that reduced phagocyte-driven inflammation supports p53EPS tumor cell

engraftment and growth. We also performed p53EPS bulk tumor cell transplantations into the hindbrain ventricles of *irf8* CRISPR/Cas9-injected syngeneic host zebrafish embryos at 2 dpf and observed 46% p53EPS tumor cell engraftment at 20 dpf, compared to 19% engraftment in *irf8* wild-type host zebrafish (p=0.0002, Fisher's exact test, Fig 5D), further supporting an inhibitory role for phagocytes within the TME. Altogether, our modeling data using patient-relevant oncogene combination in *tp53* loss-of-function background demonstrates an important role for inflammation in glioblastoma initiation and relapse including inhibitory roles for Irf-dependent signaling pathways, which in part may be attributed to anti-tumoral phagocyte activity within the TME.

Discussion

Genetically engineered mouse models (GEMM) are widely used for the study of tumorigenesis in a physiological context; however, most cannot fully recapitulate the genetic heterogeneity found in glioblastoma in a timely and cost-effective manner and are therefore limited in the context of preclinical drug testing. Patient-derived xenografts (PDX) resemble patient tumors more closely as they retain mutational heterogeneity; however, PDX models cannot be used to address mechanisms of tumor onset in an intact and endogenous tumor microenvironment given that they are derived from pre-evolved tumor tissue and are either studied *ex vivo* or engrafted into immune-deficient animal hosts. Human stem cell-derived organoids represent a great advance in the field for the study of tumor development and for screening new therapeutic strategies, but the lack of an intact TME excludes both known and unknown inter-cellular interactions, which are increasingly appreciated to influence tumor cell evolution and drug responses in patients. Therefore, to address current limitations with respect to modeling human

glioblastoma *in vivo*, we used zebrafish and neural stem/progenitor-specific expression of common oncogenic variants in a *tp53*-deficient background. We generated a robust tumor model, with a gene expression signature consistent with human glioblastoma of the mesenchymal subtype. We also harnessed the unique advantages of zebrafish modeling including *in vivo* live imaging and rapid genetic manipulations to assess characteristic inflammatory gene expression signatures within the TME, as well as roles for certain inflammatory cell types at tumor initiation and relapse following transplantation into syngeneic host animals.

Several animal models including zebrafish models of human brain cancer have been generated using transgenic overexpression of human oncogenes or xenograft transplantation of patient-derived tumor cells into immune-compromised hosts (Almstedt et al., 2022; Ju et al., 2015; Mayrhofer et al., 2017; Modzelewska et al., 2016), and these models have proven useful for defining important molecular pathways in glioma transformation, tumor growth, and cell migration. However, most of these available zebrafish models are induced using single oncogenic drivers driven by a variety of neuronal and/or glial-specific promoters at different time points throughout development, with the use of single oncogenes in a functional *tp53* signaling background potentially contributing to their inability to model highly aggressive and relapse-like phenotypes *in vivo*. Xenograft transplantations of human glioblastoma cells into zebrafish larvae omits a fully functional immune system, which our work suggests plays an important role on tumor initiation and growth both in the primary context and following p53EPS tumor cell transplantation. Therefore, our zebrafish model of aggressive and transplantable human glioblastoma represents an important opportunity to study aspects related to tumor cell progression and relapse in an intact TME.

One important consideration with model generation is use of genetic drivers that are reflective of variants found in patient tumors. $EGFR^{vIII}$ is a common genetic variant in glioblastoma that we show contributes to aggressive brain tumor formation in our zebrafish model. Interestingly, we found that our p53EPS model significantly enriches for gene expression signatures associated with mesenchymal glioblastoma, which may be unexpected given our use of $EGFR^{vIII}$ as a driver (Verhaak et al., 2010). However, from our p53EPS transcriptional signatures, we also detected expression of several markers associated with $EGFR^{vIII}$ and the classical subtype including neural progenitor and neural stem cell genes (Supplementary Fig 4, 5; Supplementary Table 1-5), potentially suggesting underlying molecular heterogeneity. In addition, histological characterization of p53EPS tumors reveal several embryonal-type features, suggesting pathological differences with respect to over-expressing human oncogenes during zebrafish development, which likely affect certain morphological features and/or gene expression patterns compared to those seen in adult glioblastoma patients. A significant amount of heterogeneity is seen in patients with respect to gene expression and histopathology, and our characterizations are consistent with certain zebrafish and rodent models using MAPK/AKT pathway activation within the developing nervous system (Huse and Holland, 2009; Jin et al., 2021; Mayrhofer et al., 2017; Wei et al., 2006). However, in the future it will be interesting to use our model and assess temporal and driver-specific contributions to specific pathohistological features and molecular subtypes at early and late stages of tumor progression, as well as inter-tumoral heterogeneity and subtype transitions to better understand how phenotypic plasticity contributes to glioblastoma growth and relapse in our model, and in patients.

Zebrafish offer a *in vivo* platform for live imaging tumor cell dynamics at high resolution, and we demonstrated a powerful model to study inter-cellular interactions during glioblastoma initiation within an endogenous TME, an approach that is not currently feasible in rodent models. The contributions of macrophages/microglia and other phagocytes to an immunosuppressive TME in glioblastoma and their prevalence within the tumor bulk is well known and has made macrophages an attractive therapeutic target for patients. For example, CSF/CSF-1R interactions have been shown to induce an immunosuppressive M2 phenotype in glioblastoma-associated microglia/macrophages, and blockade of CSF-1R improves survival in tumor burdened mice (Kennedy et al., 2013; Pyonteck et al., 2013). However, our data and work from others suggests an equally important tumor-suppressive role for microglial/macrophages based on tumor stage and activation state. For example, serial transplantation of transformed mouse neural stem cells results in strong negative pressure from the immune system in syngeneic mice, leading to activation of tumor cell-intrinsic immune evasion mechanisms that support growth *in vivo* and *in vitro* (Gangoso et al., 2021). In addition, recent spatial analyses of human glioblastoma tumor samples identified regions of activated (myeloperoxidase, MPO) macrophages that are associated with improved clinical outcomes, suggesting anti-tumorigenic roles for certain macrophage populations in patients (Karimi et al., 2023). Our modeling further supports a strong anti-tumor role for pro-inflammatory phagocytes within the endogenous TME at initiation as well as following transplantation, which is considered an experimental surrogate for relapse potential. Our data also suggests that the pro-tumorigenic immune niche seen in later-stage gliomas is not already established at initiation stages. Given that the transition to mesenchymal-like glioblastoma is closely linked to immune cell infiltration and an immune-suppressive TME (Gangoso et al., 2021; Klemm et al., 2020), it will be important to characterize these transitions to better understand anti-tumor mechanisms and their evolution during tumor

progression, with the potential for therapeutically harnessing endogenous immune cell types and/or signaling pathways in the future. Altogether, these data suggest an anti-tumor growth but potentially relapse promoting role for therapeutic anti-macrophage approaches, highlighting the importance of future *in vivo* investigations into how inhibition of transitions and/or switching immunosuppressive microglia/macrophages to immune activating states may inhibit glioblastoma growth or prevent relapse for patients. Given the role for a complexity of cell types in inflammation, it will be interesting to further assess both the innate and adaptive immune systems. For example, based on common markers we observed less evidence for neutrophils within p53EPS, consistent with the relatively low presence of neutrophils seen in human glioblastoma (Friedmann-Morvinski and Hambardzumyan, 2023). However, how these and other cell types change depending on specific genetic drivers and/or tumor stage should be highly accessible and translatable using our zebrafish model system given the broad availability of validated reporter transgenes, as well as the high level of genetic and physiological conservation with human.

Finally, it is well known that the type of glioma affects immune responses, implying that tumor-intrinsic factors shape the composition of the TME (Friebel et al., 2020; Gangoso et al., 2021; Klemm et al., 2020). Therefore, phenotypic differences with respect to glioblastoma-TME interactions in patients and model systems are likely influenced by the genetic background and oncogenic driver events. Human AKT1 over-expression in zebrafish neural cells was previously shown to drive pre-neoplastic lesions in zebrafish larvae and was found to recruit macrophage and microglia populations through the Sdf1b-Cxcr4b signaling pathway (Chia et al., 2018). In this model, loss of macrophages resulted in decreased oncogenic proliferation, suggesting tumor-promoting functions for macrophages at initiation stages. In contrast to AKT1-expressing

pre-neoplastic neurons, we visualized that neutral red-positive phagocytes and *mpeg1.1*:GFP+ macrophages/microglia very closely associated with and/or engulfed mScarlet+ p53EPS tumor cellular puncta, suggesting an effort to clear cells and/or cellular debris in p53EPS. This anti-tumor role is further supported by our functional analyses showing increased p53EPS tumor initiation in the context of Irf8 gene knock-out and decreased phagocytic cell development *in vivo* in zebrafish larvae. Given that effectively leveraging targeted therapies for glioblastoma will require a deep and individualized understanding of patient-specific tumor cell biology, it will be important to harness the flexibility of our mosaic oncogene over-expression approach and understand different tumor plus environmental factors in the context of different genetic drivers and/or modifiers identified in patients.

Methods

Zebrafish Husbandry and Care

Animals were raised in accordance with Canadian Council on Animal care (CCAC) guidelines and all experiments were approved under an Animal Use Protocol established with the Animal Care Committee at the Peter Gilgan Centre for Research and Learning (AUP #1000051391 and #1000064586). Previously described zebrafish strains including syngeneic CG1 (Mizgireuv and Revskoy, 2006), CG1tp53^{del} (Ignatius et al., 2018), Tg(*mpeg1.1*:EGFP) (Ellett et al., 2011), and Tg(*tnfa*:EGFP) (Nguyen-Chi et al., 2015) were used as indicated in the manuscript.

Preparation and injection of linearized DNA for tumorigenesis

her4.1:PI3KCA^{H1047R}, *her4.1*:mScarlet, *her4.1*:EGFR^{vIII}, *her4.1*:KRAS^{G12D}, *her4.1*:EGFP

*her4.1:*Cas9-2A-EGFP, *gfap*:EGFP, and *gfap*:mScarlet transgene expression constructs were cloned using previously described *her4.1* sequence (Yeo et al., 2007) , *gfap* entry plasmid (Don et al., 2017), standard Tol2 Gateway plasmids and protocols (Kwan et al., 2007). *rag2*:EGFP and *mpeg1.1*:EGFP expression plasmids were previously described (Ellett et al., 2011; Langenau et al., 2007). Circular *her4.1* expression plasmids were linearized using XhoI restriction enzyme (New England Biolabs, R0146S) while *gfap*:EGFP was linearized using ClaI (New England Biolabs, R0197S), according to manufacturer's protocol. Restriction enzymes were heat inactivated and linearized vector purified utilizing an EZ-10 Spin Column PCR Products Purification Kit (Bio Basic, BS364). Injection mixtures such as EPS (*her4.1*:**E**GFR^{vIII}, *her4.1*:**P**I3KCA^{H1047R}, *her4.1*:m**S**carlet) or KPG (*her4.1*:**K**RAS, *her4.1*:**P**I3KCA^{H1047R}, *her4.1*:**G**FP) were prepared at 2:1:1 molar ratios in 50% TE Buffer (Invitrogen, 12090-015) with KCl (final concentration 0.1M) and Phenol red (final concentration 5%, Sigma-Aldrich, P0290). CG1 or CG1tp53^{del} embryos were micro injected with 0.5-1nL of injection mixture at the one-cell stage and monitored for tumor development, starting at 10-15 days post fertilization (dpf).

Guide RNA Synthesis and CRISPR-Cas9-Mediated Gene Targeting

CRISPR/Cas9 sequence targets and guide RNA (gRNA) oligos were designed using CHOPCHOP (Labun et al., 2019). Guide RNA were *in vitro* synthesized using the EnGen sgRNA Synthesis Kit (New England Biolabs, E3322V) cording to manufacturer's recommendation. Cas9 protein with NLS (PNA Bio, CP01-200) was resuspended in 20% glycerol/water to a concentration of 1mg/ml. Cas9/gRNA microinjection mix was prepared at a final concentration of 0.3mg/ml Cas9 + 30-50ng/ul of each gRNA. 0.5-1nL of injection mix and injected into zebrafish embryos of the indicated genotype, at the one-cell stage. CRISPR/Cas9 targeting efficiency was measured following PCR-based locus amplification, Sanger sequencing

and Synthego ICE Analysis (ICE analysis, Synthego, ice.synthego.com) (Synthego, 2019). All gRNA sequences and PCR oligos are indicated in Supplementary Table 7.

Brain Dissection and Dissociation

Animals were euthanized with a lethal 300mg/L dose of tricaine (Sigma-Aldrich, E10521) ~10-20 minutes before dissection. Fish were decapitated posterior of the gills and the head transferred to sterile-filtered PBS (Wisent Inc., 311-010-CL). Using fine-tipped forceps, brains were carefully extracted from the skull and transferred to a micro centrifuge tube and kept in PBS at 28°C until further processing. 5-10 brains were transferred to 1ml of 28°C pre-warmed Accutase (Stemcell, 07920), followed by incubation at 28°C with gentle rocking for a total of ~50 minutes. Every 10 minutes, brains were mechanically dissociated with gentle pipetting 15-30 times using a 1mL filter tip. Dissociated tissues were passed through a 40um Cell Strainer (Corning, 352340) into a 50ml conical tube to achieve single cell suspensions. Strained cells were pelleted at approximately 1000 x g for 5 minutes at room temperature and resuspended in PBS.

Bulk Tumor Cell Transplantation

Cell suspensions were maintained at 28°C during the transplantation procedure. 2dpf CG1 strain syngeneic zebrafish larvae were injected with 1-2nL of cell suspension into the hindbrain ventricle, as previously described (Casey et al., 2017). Cells were injected alone or in combination with 1% total volume Clodrosomes (Encapsula Nano Sciences, CLD-8901), vehicle control liposomes, or 0.05ng/nL human CSF-1 recombinant protein (Cell Signaling Technology, 8929SC).

Immunohistochemistry and Fluorescent *in situ* Hybridization (FISH)

Zebrafish were fixed overnight in 4% PFA and stored in methanol at -20°C before paraffin embedding and sectioning at the Centre for Phemogenomics Pathology Core Facility. Animal sections were deparaffinized with 2x5 minute washes of Xylenes. Sections were rehydrated with sequential 2x10 minute washes in 100%, 90%, 70% ethanol before sequential rinsing with ddH20, 3% H_2O_2, and ddH20. Slides were then boiled in 1x Citrate Buffer (Sigma-Aldrich, C999) within a standard microwave and rinsed in ddH20, after cooling for 30 minutes. Sections were blocked with TBST/5% Normal Goat Serum for 1 hour at RT before overnight incubation with primary antibody diluted in Diluent CST (Cell Signaling Technology, 8112) at 4°C. The following day slides were washed once with 3x5 minutes with TBS, TBST, and TBS. Samples were then incubated with secondary antibody (Cell Signaling Technology, 8114) for half an hour at room temperature, followed by another 3x5 minute TBS/T wash. Standard DAB development (Thermo Scientific, 34002) was performed for 5-7 minutes, followed by water termination. Samples were Hematoxylin (VWR, 10143-146) stained with a 1:6 diluted solution for 3-5 seconds and rinsed 5x with tap water. Slides were dehydrated sequentially with 70%, 90%, 100% ethanol washes followed by 2x5 minute Xylene washes before being mounted with glass cover slips and Permount (Fisher Scientific, SP15-100). Primary antibodies raised against proliferating cell nuclear antigen (PCNA, Cell Signaling, D3H8P), phosphorylated ERK (Cell Signaling, #9101) and phosphorylated AKT (Cell Signaling, #9271) were used.

Whole mount FISH was performed on fixed larvae using *EGFP* and *irf7*-specific antisense probes (Molecular Instruments) and HCR protocol, according to manufacturer's recommendations.

Bulk RNASeq Library Preparation, Quantification and Differential Gene Expression Analysis

Three p53KPG, p53EPS, and control-injected brains (from non-tumor forming injected siblings) were harvested at 20-30 dpf and immediately placed into 1mL of TRIzol Reagent (Invitrogen, 15596026). mScarlet+ tumor cells were also sorted from bulk (non-fluorescent) tissue from pooled brains at the SickKids-UHN Flow Cytometry Core Facility on a Sony MA900 VBYR cell sorter, before pelleting and lysis in TRIzol Reagent. Total RNA was purified for all samples using a Monarch RNA Cleanup Kit (New England Biolabs, T2040L), according to manufacturer's recommendations. Sequence ready polyA-enriched libraries were prepared using the NEB Ultra II Directional mRNA prep kit for Illumina (NEB, E7760), according to manufacturer's recommendations. Single-end 150bp sequencing at a targeted depth of ~30-60 million reads/sample was performed using an Illumina NovaSeq S1 flowcell, at the Centre for Applied Genomics (TCAG). Raw .fastq data was processed using Salmon quantification of transcripts for each sample. A "decoy-aware" index was built with the *Danio rerio* transcriptome and genome using the GRCz11 assembly with a k-mers length of 23. Samples were then quantified with the following arguments: -r, --seqBias, --mp -3, --validateMappings, --rangeFactorizationBins 4. Sequencing data is available from GEO under accession code GSE246295.

Human Ortholog Conversion and GSEA

Normalized counts output from DESeq2 for the above processed data were utilized for GSEA analysis without any further trimming or processing, as recommend by the GSEA user guide (Mootha et al., 2003; Subramanian et al., 2005). Zebrafish transcripts were assigned known or high-confidence Human orthologs using Ensembl BioMart, as previously described (Demirci et

al., 2022). Bulk sequencing data from *her4.1:*KRAS^{G12D} or *her4.1:*EGFR^{viii} driven tumors, or sorted cells derived from such, were compared with non-tumour control brains under default conditions (1000 permutations, gene set). Expression signatures were compared against published glioblastoma (McLendon et al., 2008; Wang et al., 2017), medulloblastoma (Cavalli et al., 2017), Hallmark and/or C7: immunologic signature gene sets (Liberzon et al., 2011), as indicated in the manuscript.

Neutral Red Staining and Quantification

Zebrafish were treated with Neutral Red, as previously described (Shiau et al., 2013). Animals were then anesthetized in Tricaine and oriented on their sides in 3% methylcellulose before an image stack of approximately 120-150um depth was taken beginning from the surface of the otic vesicle into the fish. Neutral Red stained foci were counted using Zen Lite Software (version 3.3) in an area bounded by the posterior edge of the eye and the posterior edge of the otic vesicle for each fish.

Image Acquisition

Fluorescence and bright field image acquisition of whole animals and dissected tumor-burdened brains was performed using a Zeiss Axiozoom V16 macroscope. High resolution confocal microscopy was performed using a Nikon 1AR confocal microscope, with image processing and Z-stack compression performed using ImageJ software. IHC slides were imaged on a Pannoramic Flash II.

RT-qPCR and Analysis

Total RNA was extracted from tumor-burdened brains using TRIzol reagent, as described above, and reverse transcribed using the High-Capacity DNA Reverse Transcriptase Kit (Thermo Fisher, 4368814), as per manufacturer's recommendations. RT-qPCR was performed using the SYBR Green I Master kit (Roche, 04887352001) following the manufacturer's recommended protocol and a Bio-Rad CFX96 qPCR Real-Time PCR Module with C1000 Touch Termal Cycler Unit. All primers used to amplify genes of interest are indicated in Supplementary Table 7. At least 5 brain samples were pooled for each sample, with gene expression normalized to *18s*. Where indicated, gene expression was normalized to *mScarlet* expression to control for differences in overall tumor size.

Data Availability

All sequencing data is deposited in NCBI GEO under accession code GSE246295: https://www.ncbi.nlm.nih.gov/geo/query/acc.cgi?acc=GSE246295.

Acknowledgements: We thank Dr. David Langenau for CG1*tp53*^{del} zebrafish. We also thank the Centre for Phenogenomics (TCP) Histopathology core for tissue processing and staining, the Centre for Applied Genomics (TCAG) for sequencing, the SickKids Imaging Facility, and the Zebrafish Genetics and Disease Models Facility management and support team for zebrafish husbandry. We thank Dr. Matt Wood at Oregon Health & Science University for pathology on zebrafish brain tumors.

Financial Support: BJP and AW were supported by Ontario Institute for Cancer Research (OICR) operating grant IA-026. CD was supported by Canadian Institutes of Health Research

(CIHR) Grant # PJT-159611. BJP was supported by OHSU startup funds. MNH was supported by a CIHR postdoctoral fellowship, startup funds from the Hospital for Sick Children, and the Hospital for Sick Children Foundation.

References

Aldape K, Brindle KM, Chesler L, Chopra R, Gajjar A, Gilbert MR, Gottardo N, Gutmann DH, Hargrave D, Holland EC, Jones DTW, Joyce JA, Kearns P, Kieran MW, Mellinghoff IK, Merchant M, Pfister SM, Pollard SM, Ramaswamy V, Rich JN, Robinson GW, Rowitch DH, Sampson JH, Taylor MD, Workman P, Gilbertson RJ. 2019. Challenges to curing primary brain tumours. *Nat Rev Clin Oncol* 16:509–520.

Almstedt E, Rosen E, Gloger M, Stockgard R, Hekmati N, Koltowska K, Krona C, Nelander S. 2022. Real-time evaluation of glioblastoma growth in patient-specific zebrafish xenografts. *Neuro Oncol* 24:726–738.

Andreou KE, Soto MS, Allen D, Economopoulos V, de Bernardi A, Larkin JR, Sibson NR. 2017. Anti-inflammatory microglia/macrophages as a potential therapeutic target in brain metastasis. *Front Oncol* 7:251.

Bikfalvi A, da Costa CA, Avril T, Barnier JV, Bauchet L, Brisson L, Cartron PF, Castel H, Chevet E, Chneiweiss H, Clavreul A, Constantin B, Coronas V, Daubon T, Dontenwill M, Ducray F, Enz-Werle N, Figarella-Branger D, Fournier I, Frenel JS, Gabut M, Galli T, Gavard J, Huberfeld G, Hugnot JP, Idbaih A, Junier MP, Mathivet T, Menei P, Meyronet D, Mirjolet C, Morin F, Mosser J, Moyal ECJ, Rousseau V, Salzet M, Sanson M, Seano G, Tabouret E, Tchoghandjian A, Turchi L, Vallette FM, Vats S, Verreault M, Virolle T. 2023. Challenges in glioblastoma research: focus on the tumor microenvironment. *Trends Cancer* 9:9-27.

Biswas SK, Sica A, Lewis CE. 2008. IMMUNOLOGY Plasticity of Macrophage Function during Tumor Progression: Regulation by Distinct Molecular Mechanisms 1, The Journal of Immunology. 2011-2017.

Blackburn JS, Liu S, Langenau DM. 2011. Quantifying the frequency of tumor-propagating cells using limiting dilution cell transplantation in syngeneic zebrafish. *Journal of Visualized Experiments*. e2790.

Brennan CW, Verhaak RGW, McKenna A, Campos B, Noushmehr H, Salama SR, Zheng S, Chakravarty D, Sanborn JZ, Berman SH, Beroukhim R, Bernard B, Wu CJ, Genovese G, Shmulevich I, Barnholtz-Sloan J, Zou L, Vegesna R, Shukla SA, Ciriello G, Yung WKA, Zhang W, Sougnez C, Mikkelsen T, Aldape K, Bigner DD, Van Meir EG, Prados M, Sloan AE, Black

KL, Eschbacher J, Finocchiaro G, Friedman W, Andrews DW, Guha A, Iacocca M, O'Neill BP, Foltz G, Myers J, Weisenberger DJ, Penny R, Kucherlapati R, Perou CM, Hayes DN, Gibbs R, Marra M, Mills GB, Lander ES, Spellman P, Wilson R, Sander C, Weinstein J, Meyerson M, Gabriel S, Laird PW, Haussler D, Getz G, Chin L, Benz C, Barrett W, Ostrom Q, Wolinsky Y, Bose B, Boulos PT, Boulos M, Brown J, Czerinski C, Eppley M, Kempista T, Kitko T, Koyfman Y, Rabeno B, Rastogi P, Sugarman M, Swanson P, Yalamanchii K, Otey IP, Liu YS, Xiao Y, Auman JT, Chen PC, Hadjipanayis A, Lee E, Lee S, Park PJ, Seidman J, Yang Lixing, Kalkanis S, Poisson LM, Raghunathan A, Scarpace L, Bressler R, Eakin A, Iype L, Kreisberg RB, Leinonen K, Reynolds S, Rovira H, Thorsson V, Annala MJ, Paulauskis J, Curley E, Hatfield M, Mallery D, Morris S, Shelton T, Shelton C, Sherman M, Yena P, Cuppini L, DiMeco F, Eoli M, Maderna E, Pollo B, Saini M, Balu S, Hoadley KA, Li L, Miller CR, Shi Y, Topal MD, Wu J, Dunn G, Giannini C, Aksoy BA, Antipin Y, Borsu L, Cerami E, Gao J, Gross B, Jacobsen A, Ladanyi M, Lash A, Liang Y, Reva B, Schultz N, Shen R, Socci ND, Viale A, Ferguson ML, Chen QR, Demchok JA, Dillon LAL, Mills Shaw KR, Sheth M, Tarnuzzer R, Wang Z, Yang Liming, Davidsen T, Guyer MS, Ozenberger BA, Sofia HJ, Bergsten J, Eckman J, Harr J, Smith C, Tucker K, Winemiller C, Zach LA, Ljubimova JY, Eley G, Ayala B, Jensen MA, Kahn A, Pihl TD, Pot DA, Wan Y, Hansen N, Hothi P, Lin B, Shah N, Yoon JG, Lau C, Berens M, Ardlie K, Carter SL, Cherniack AD, Noble M, Cho J, Cibulskis K, DiCara D, Frazer S, Gabriel SB, Gehlenborg N, Gentry J, Heiman D, Kim J, Jing R, Lawrence M, Lin P, Mallard W, Onofrio RC, Saksena G, Schumacher S, Stojanov P, Tabak B, Voet D, Zhang H, Dees NN, Ding L, Fulton LL, Fulton RS, Kanchi KL, Mardis ER, Wilson RK, Baylin SB, Harshyne L, Cohen ML, Devine K, Van Den Berg SR, Berger MS, Carlin D, Craft B, Ellrott K, Goldman M, Goldstein T, Grifford M, Ma S, Ng S, Stuart J, Swatloski T, Waltman P, Zhu J, Foss R, Frentzen B, McTiernan R, Yachnis A, Mao Y, Akbani R, Bogler O, Fuller GN, Liu W, Liu Y, Lu Y, Protopopov A, Ren X, Sun Y, Zhang J, Chen K, Weinstein JN, Bootwalla MS, Lai PH, Triche TJ, Van Den Berg DJ, Gutmann DH, Lehman NL, Brat D, Olson JJ, Mastrogianakis GM, Devi NS, Zhang Z, Lipp E, McLendon R. 2013. The somatic genomic landscape of glioblastoma. *Cell* 155:462.

Casey MJ, Modzelewska K, Anderson D, Goodman J, Boer EF, Jimenez L, Grossman D, Stewart RA. 2017. Transplantation of Zebrafish pediatric brain tumors into immune-competent hosts for long-term study of tumor cell behavior and drug response. *Journal of Visualized Experiments*. 55712.

Cavalli FMG, Remke M, Rampasek L, Peacock J, Shih DJH, Luu B, Garzia L, Torchia J, Nor C, Morrissy AS, Agnihotri S, Thompson YY, Kuzan-Fischer CM, Farooq H, Isaev K, Daniels C, Cho BK, Kim SK, Wang KC, Lee JY, Grajkowska WA, Perek-Polnik M, Vasiljevic A, Faure-Conter C,

Jouvet A, Giannini C, Nageswara Rao AA, Li KKW, Ng HK, Eberhart CG, Pollack IF, Hamilton RL, Gillespie GY, Olson JM, Leary S, Weiss WA, Lach B, Chambless LB, Thompson RC, Cooper MK, Vibhakar R, Hauser P, van Veelen MLC, Kros JM, French PJ, Ra YS, Kumabe T, López-Aguilar E, Zitterbart K, Sterba J, Finocchiaro G, Massimino M, Van Meir EG, Osuka S, Shofuda T, Klekner A, Zollo M, Leonard JR, Rubin JB, Jabado N, Albrecht S, Mora J, Van Meter TE, Jung S, Moore AS, Hallahan AR, Chan JA, Tirapelli DPC, Carlotti CG, Fouladi M, Pimentel J, Faria CC, Saad AG, Massimi L, Liau LM, Wheeler H, Nakamura H, Elbabaa SK, Perezpeña-Diazconti M, Chico Ponce de León F, Robinson S, Zapotocky M, Lassaletta A, Huang A, Hawkins CE, Tabori U, Bouffet E, Bartels U, Dirks PB, Rutka JT, Bader GD, Reimand J, Goldenberg A, Ramaswamy V, Taylor MD. 2017. Intertumoral Heterogeneity within Medulloblastoma Subgroups. *Cancer Cell* 31:737-754.

Chen X, Wanggou S, Bodalia A, Zhu M, Dong W, Fan JJ, Yin WC, Min HK, Hu M, Draghici D, Dou W, Li F, Coutinho FJ, Whetstone H, Kushida MM, Dirks PB, Song Y, Hui C chung, Sun Y, Wang LY, Li X, Huang X. 2018. A Feedforward Mechanism Mediated by Mechanosensitive Ion Channel PIEZO1 and Tissue Mechanics Promotes Glioma Aggression. *Neuron* 100:799-815.

Chen Y, Huo R, Kang W, Liu Y, Zhao Z, Fu W, Ma R, Zhang X, Tang J, Zhu Z, Lyu Q, Huang Y, Yan M, Jiang B, Chai R, Bao Z, Hu Z, Wang W, Jiang T, Cao Y, Wang J. 2023. Tumor-associated monocytes promote mesenchymal transformation through EGFR signaling in glioma. *Cell Rep Med* 4:101177.

Chia K, Mazzolini J, Mione M, Sieger D. 2018. Tumor initiating cells induce Cxcr4-mediated infiltration of pro-tumoral macrophages into the brain. *Elife* 7:e31918.

Couturier CP, Ayyadhury S, Le PU, Nadaf J, Monlong J, Riva G, Allache R, Baig S, Yan X, Bourgey M, Lee C, Wang YCD, Wee Yong V, Guiot MC, Najafabadi H, Misic B, Antel J, Bourque G, Ragoussis J, Petrecca K. 2020. Single-cell RNA-seq reveals that glioblastoma recapitulates a normal neurodevelopmental hierarchy. *Nat Commun* 11:3406.

Darmanis S, Sloan SA, Croote D, Mignardi M, Chernikova S, Samghababi P, Zhang Y, Neff N, Kowarsky M, Caneda C, Li G, Chang SD, Connolly ID, Li Y, Barres BA, Gephart MH, Quake SR. 2017. Single-Cell RNA-Seq Analysis of Infiltrating Neoplastic Cells at the Migrating Front of Human Glioblastoma. *Cell Rep* 21:1399–1410.

Demirci Y, Heger G, Katkat E, Papatheodorou I, Brazma A, Ozhan G. 2022. Brain Regeneration Resembles Brain Cancer at Its Early Wound Healing Stage and Diverges From Cancer Later at Its Proliferation and Differentiation Stages. *Front Cell Dev Biol* 10:813314.

Don EK, Formella I, Badrock AP, Hall TE, Morsch M, Hortle E, Hogan A, Chow S, Gwee SSL, Stoddart JJ, Nicholson G, Chung R, Cole NJ. 2017. A Tol2 Gateway-Compatible Toolbox for the Study of the Nervous System and Neurodegenerative Disease. *Zebrafish* 14:69–72.

Ellett F, Pase L, Hayman JW, Andrianopoulos A, Lieschke GJ. 2011. Mpeg1 Promoter Transgenes Direct Macrophage-Lineage Expression in Zebrafish. *Blood* 117:49–56.
Feng H, Zhang Q-M, Zhang Y-B, Li Z, Zhang J, Xiong Y-W, Wu M, Gui J-F. 2016. Zebrafish IRF1, IRF3, and IRF7 Differentially Regulate IFNΦ1 and IFNΦ3 Expression through Assembly of Homo- or Heteroprotein Complexes. *The Journal of Immunology* 197:1893–1904.

Friebel E, Kapolou K, Unger S, Núñez NG, Utz S, Rushing EJ, Regli L, Weller M, Greter M, Tugues S, Neidert MC, Becher B. 2020. Single-Cell Mapping of Human Brain Cancer Reveals Tumor-Specific Instruction of Tissue-Invading Leukocytes. *Cell* 181:1626-1642
Friebel E, Kapolou K, Unger S, Núñez NG, Utz S, Rushing EJ, Regli L, Weller M, Greter M, Tugues S, Neidert MC, Becher B. 2020. Single-Cell Mapping of Human Brain Cancer Reveals Tumor-Specific Instruction of Tissue-Invading Leukocytes. *Cell* 181:1626-1642.
Friedmann-Morvinski D, Hambardzumyan D. 2023. Monocyte-neutrophil entanglement in glioblastoma. *Journal of Clinical Investigation* 133:e163451.

Gangoso E, Southgate B, Bradley L, Rus S, Galvez-Cancino F, McGivern N, Güç E, Kapourani CA, Byron A, Ferguson KM, Alfazema N, Morrison G, Grant V, Blin C, Sou IF, Marques-Torrejon MA, Conde L, Parrinello S, Herrero J, Beck S, Brandner S, Brennan PM, Bertone P, Pollard JW, Quezada SA, Sproul D, Frame MC, Serrels A, Pollard SM. 2021. Glioblastomas acquire myeloid-affiliated transcriptional programs via epigenetic immunoediting to elicit immune evasion. *Cell* 184:2454-2470.

Gómez-Oliva R, Domínguez-García S, Carrascal L, Abalos-Martínez J, Pardillo-Díaz R, Verástegui C, Castro C, Nunez-Abades P, Geribaldi-Doldán N. 2021. Evolution of Experimental Models in the Study of Glioblastoma: Toward Finding Efficient Treatments. *Front Oncol* 10:614295.

Günthner R, Anders HJ. 2013. Interferon-regulatory factors determine macrophage phenotype polarization. *Mediators Inflamm* 2013:731023.

Gutmann DH, Kettenmann H. 2019. Microglia/Brain Macrophages as Central Drivers of Brain Tumor Pathobiology. *Neuron* 104:442-449.

Haddad AF, Young JS, Amara D, Berger MS, Raleigh DR, Aghi MK, Butowski NA. 2021. Mouse models of glioblastoma for the evaluation of novel therapeutic strategies. *Neurooncol Adv* 3:1–16.

Hanlon LA, Raghupathi R, Huh JW. 2019. Depletion of microglia immediately following traumatic brain injury in the pediatric rat: Implications for cellular and behavioral pathology. *Exp Neurol* 316:39–51.

Hao NB, Lü MH, Fan YH, Cao YL, Zhang ZR, Yang SM. 2012. Macrophages in tumor microenvironments and the progression of tumors. *Clin Dev Immunol* 2012:948098.

Hayes MN, McCarthy KM, Jin A, Oliveira ML, Iyer S, Garcia SP, Sindiri S, Gryder B, Motala Z, Nielsen GP, Borg J-P, van de Rijn M, Malkin D, Khan J, Ignatius MS, Langenau DM. 2018. Vangl2 regulates stem cell self-renewal programs and growth in Rhabdomyosarcoma through a Wnt/PCP/RhoA signaling axis. *Cell Stem Cell* 22:414–427.

Herbomel P, Thisse B, Thisse C. 2001. Zebrafish early macrophages colonize cephalic mesenchyme and developing brain, retina, and epidermis through a M-CSF receptor-dependent invasive process. *Dev Biol* 238:274–288.

Holland JD, Klaus A, Garratt AN, Birchmeier W. 2013. Wnt signaling in stem and cancer stem cells. *Curr Opin Cell Biol* 25:254–264.

Hoogstrate Y, Ghisai SA, De Wit M, De Heer I, Draaisma K, Van Riet J, Van De Werken HJG, Bours V, Buter J, Vanden Bempt I, Eoli M, Franceschi E, Frenel JS, Gorlia T, Hanse MC, Hoeben A, Kerkhof M, Kros JM, Leenstra S, Lombardi G, Lukacova S, Robe PA, Sepulveda JM, Taal W, Taphoorn M, Vernhout RM, Walenkamp AME, Watts C, Weller M, De Vos FYF, Jenster GW, Van Den Bent M, French PJ. 2022. The EGFRvIII transcriptome in glioblastoma: A meta-omics analysis. *Neuro Oncol* 24:429–441.

Hu SQ, Xu HM, Qian FP, Chen CS, Wang X, Liu D, Cheng L. 2022. Interferon regulatory factor-7 is required for hair cell development during zebrafish embryogenesis. *Dev Neurobiol* 82:88–97.

Huse JT, Holland EC. 2009. Genetically engineered mouse models of brain cancer and the promise of preclinical testing. *Brain Pathol* 19:132–143.

Ignatius MS, Hayes MN, Lobbardi R, Chen EY, McCarthy KM, Sreenivas P, Motala Z, Durbin AD, Molodtsov A, Reeder S, Jin A, Sindiri S, Beleyea BC, Bhere D, Alexander MS, Shah K, Keller C, Linardic CM, Nielsen PG, Malkin D, Khan J, Langenau DM. 2017. The NOTCH1/SNAIL1/MEF2C Pathway Regulates Growth and Self-Renewal in Embryonal Rhabdomyosarcoma. *Cell Rep* 19:2304–2318.

Ignatius MS, Hayes MN, Moore FE, Tang Q, Garcia SP, Blackburn PR, Baxi K, Wang L, Jin A, Ramakrishnan A, Reeder S, Chen Y, Nielsen GP, Chen EY, Hasserjian RP, Tirode F, Ekker SC, Langenau DM. 2018. Tp53 deficiency causes a wide tumor spectrum and increases embryonal rhabdomyosarcoma metastasis in zebrafish. *Elife* 7:e37202.
Jin F, Jin-Lee HJ, Johnson AJ. 2021. Mouse Models of Experimental Glioblastoma In: Gliomas. Exon Publications.

Jin X, Kim Sung Hak, Jeon HM, Beck S, Sohn YW, Yin J, Kim JK, Lim YC, Lee JH, Kim Se Hyuk, Kang SH, Pian X, Song MS, Park JB, Chae YS, Chung YG, Lee SH, Choi YJ, Nam DH, Choi YK, Kim H. 2012. Interferon regulatory factor 7 regulates glioma stem cells via interleukin-6 and Notch signalling. *Brain* 135:1055–1069.

Ju B, Chen W, Orr BA, Spitsbergen JM, Jia S, Eden CJ, Henson HE, Taylor MR. 2015. Oncogenic KRAS promotes malignant brain tumors in zebrafish. *Mol Cancer* 14:18.
Kaffes I, Szulzewsky F, Chen Z, Herting CJ, Gabanic B, Velázquez Vega JE, Shelton J, Switchenko JM, Ross JL, McSwain LF, Huse JT, Westermark B, Nelander S, Forsberg-Nilsson K, Uhrbom L, Maturi NP, Cimino PJ, Holland EC, Kettenmann H, Brennan CW, Brat DJ, Hambardzumyan D. 2019. Human Mesenchymal glioblastomas are characterized by an increased immune cell presence compared to Proneural and Classical tumors. *Oncoimmunology* 8:e1655360.

Karimi E, Yu MW, Maritan SM, Perus LJM, Rezanejad M, Sorin M, Dankner M, Fallah P, Doré S, Zuo D, Fiset B, Kloosterman DJ, Ramsay LA, Wei Y, Lam S, Alsajjan R, Watson IR, Roldan

Urgoiti G, Park M, Brandsma D, Senger DL, Chan JA, Akkari L, Petrecca K, Guiot MC, Siegel PM, Quail DF, Walsh LA. 2023. Single-cell spatial immune landscapes of primary and metastatic brain tumours. *Nature* 614:555–563.

Karperien A, Ahammer H, Jelinek HF. 2013. Quantitating the subtleties of microglial morphology with fractal analysis. *Front Cell Neurosci*. Jan 30:7:3.

Kennedy BC, Showers CR, Anderson DE, Anderson L, Canoll P, Bruce JN, Anderson RCE. 2013. Tumor-associated macrophages in glioma: Friend or foe? *J Oncol* 2013:486912.

Khan F, Pang L, Dunterman M, Lesniak MS, Heimberger AB, Chen P. 2023. Macrophages and microglia in glioblastoma: heterogeneity, plasticity, and therapy. *Journal of Clinical Investigation*. 133:e163446.

Klemm F, Maas RR, Bowman RL, Kornete M, Soukup K, Nassiri S, Brouland JP, Iacobuzio-Donahue CA, Brennan C, Tabar V, Gutin PH, Daniel RT, Hegi ME, Joyce JA. 2020. Interrogation of the Microenvironmental Landscape in Brain Tumors Reveals Disease-Specific Alterations of Immune Cells. *Cell* 181:1643-1660.e17.

Kwan KM, Fujimoto E, Grabher C, Mangum BD, Hardy ME, Campbell DS, Parant JM, Yost HJ, Kanki JP, Chien C Bin. 2007. The Tol2kit: A multisite gateway-based construction Kit for Tol2 transposon transgenesis constructs. *Developmental Dynamics* 236:3088–3099.
Labun K, Montague TG, Krause M, Torres Cleuren YN, Tjeldnes H, Valen E. 2019.

CHOPCHOP v3: Expanding the CRISPR web toolbox beyond genome editing. *Nucleic Acids Res* 47:W171–W174.

Langenau DM, Keefe MD, Storer NY, Guyon JR, Kutok JL, Le X, Goessling W, Neuberg DS, Kunkel LM, Zon LI. 2007. Effects of RAS on the genesis of embryonal rhabdomyosarcoma. *Genes Dev* 21:1382–95.

Langenau DM, Keefe MD, Storer NY, Jette CA, Smith ACH, Ceol CJ, Bourque C, Look AT, Zon LI. 2008. Co-injection strategies to modify radiation sensitivity and tumor initiation in transgenic Zebrafish. *Oncogene* 27:4242–4248.

Liberzon A, Subramanian A, Pinchback R, Thorvaldsdóttir H, Tamayo P, Mesirov JP. 2011. Molecular signatures database (MSigDB) 3.0. *Bioinformatics* 27:1739–1740.
Majc B, Sever T, Zarić M, Breznik B, Turk B, Lah TT. 2020. Epithelial-to-mesenchymal transition as the driver of changing carcinoma and glioblastoma microenvironment. *Biochim Biophys Acta Mol Cell Res*. 1867:118782.

Mayrhofer M, Gourain V, Reischl M, Affaticati P, Jenett A, Joly JS, Benelli M, Demichelis F, Poliani PL, Sieger D, Mione M. 2017. A novel brain tumour model in zebrafish reveals the role of YAP activation in MAPK- and PI3K-induced malignant growth. *DMM Disease Models and Mechanisms* 10:15–28.

McGranahan T, Therkelsen KE, Ahmad S, Nagpal S. 2019. Current State of Immunotherapy for Treatment of Glioblastoma. *Curr Treat Options Oncol*. 20:24.

McLendon R, Friedman A, Bigner D, Van Meir EG, Brat DJ, Mastrogianakis GM, Olson JJ, Mikkelsen T, Lehman N, Aldape K, Yung WKA, Bogler O, Weinstein JN, VandenBerg S, Berger M, Prados M, Muzny D, Morgan M, Scherer S, Sabo A, Nazareth L, Lewis L, Hall O, Zhu Y, Ren Y, Alvi O, Yao Jiqiang, Hawes A, Jhangiani S, Fowler G, San Lucas A, Kovar C, Cree A, Dinh H, Santibanez J, Joshi V, Gonzalez-Garay ML, Miller CA, Milosavljevic A, Donehower L, Wheeler DA, Gibbs RA, Cibulskis K, Sougnez C, Fennell T, Mahan S, Wilkinson J, Ziaugra L, Onofrio R, Bloom T, Nicol R, Ardlie K, Baldwin J, Gabriel S, Lander ES, Ding L, Fulton RS, McLellan MD, Wallis J, Larson DE, Shi X, Abbott R, Fulton L, Chen K, Koboldt DC, Wendl MC, Meyer R, Tang Y, Lin L, Osborne JR, Dunford-Shore BH, Miner TL, Delehaunty K, Markovic C, Swift G, Courtney W, Pohl C, Abbott S, Hawkins A, Leong S, Haipek C, Schmidt H, Wiechert M, Vickery T, Scott S, Dooling DJ, Chinwalla A, Weinstock GM, Mardis ER, Wilson RK, Getz G, Winckler W, Verhaak RGW, Lawrence MS, O'Kelly M, Robinson J, Alexe G, Beroukhim R, Carter S, Chiang D, Gould J, Gupta S, Korn J, Mermel C, Mesirov J, Monti S, Nguyen H, Parkin M, Reich M, Stransky N, Weir BA, Garraway L, Golub T, Meyerson M, Chin L, Protopopov A, Zhang Jianhua, Perna I, Aronson S, Sathiamoorthy N, Ren G, Yao Jun, Wiedemeyer WR, Kim H, Sek WK, Xiao Y, Kohane IS, Seidman J, Park PJ, Kucherlapati R, Laird PW, Cope L, Herman JG, Weisenberger DJ, Pan F, Van Den Berg D, Van Neste L, Joo MY, Schuebel KE, Baylin SB, Absher DM, Li JZ, Southwick A, Brady S, Aggarwal A, Chung T, Sherlock G, Brooks JD, Myers RM, Spellman PT, Purdom E, Jakkula LR, Lapuk A V., Marr H, Dorton S, Yoon GC, Han J, Ray A, Wang V, Durinck S, Robinson M, Wang NJ, Vranizan K, Peng V, Van Name E, Fontenay G V., Ngai J, Conboy JG, Parvin B, Feiler HS, Speed TP, Gray JW, Brennan C, Socci ND, Olshen A, Taylor BS, Lash A, Schultz N, Reva B, Antipin Y, Stukalov A, Gross B, Cerami E,

Wei QW, Qin LX, Seshan VE, Villafania L, Cavatore M, Borsu L, Viale A, Gerald W, Sander C, Ladanyi M, Perou CM, Hayes DN, Topal MD, Hoadley KA, Qi Y, Balu S, Shi Y, Wu J, Penny R, Bittner M, Shelton T, Lenkiewicz E, Morris S, Beasley D, Sanders S, Kahn A, Sfeir R, Chen J, Nassau D, Feng L, Hickey E, Barker A, Gerhard DS, Vockley J, Compton C, Vaught J, Fielding P, Ferguson ML, Schaefer C, Zhang Jinghui, Madhavan S, Buetow KH, Collins F, Good P, Guyer M, Ozenberger B, Peterson J, Thomson E. 2008. Comprehensive genomic characterization defines human glioblastoma genes and core pathways. *Nature* 455:1061–1068.

Mizgireuv I V., Revskoy SY. 2006. Transplantable tumor lines generated in clonal zebrafish. *Cancer Res* 66:3120–3125.

Modzelewska K, Boer EF, Mosbruger TL, Picard D, Anderson D, Miles RR, Kroll M, Oslund W, Pysher TJ, Schiffman JD, Jensen R, Jette CA, Huang A, Stewart RA. 2016. MEK Inhibitors Reverse Growth of Embryonal Brain Tumors Derived from Oligoneural Precursor Cells. *Cell Rep* 17:1255–1264.

Mootha VK, Lindgren CM, Eriksson KF, Subramanian A, Sihag S, Lehar J, Puigserver P, Carlsson E, Ridderstråle M, Laurila E, Houstis N, Daly MJ, Patterson N, Mesirov JP, Golub TR, Tamayo P, Spiegelman B, Lander ES, Hirschhorn JN, Altshuler D, Groop LC. 2003. PGC-1α-responsive genes involved in oxidative phosphorylation are coordinately downregulated in human diabetes. *Nat Genet* 34:267-273.

Neftel C, Laffy J, Filbin MG, Hara T, Shore ME, Rahme GJ, Richman AR, Silverbush D, Shaw ML, Hebert CM, Dewitt J, Gritsch S, Perez EM, Gonzalez Castro LN, Lan X, Druck N, Rodman C, Dionne D, Kaplan A, Bertalan MS, Small J, Pelton K, Becker S, Bonal D, Nguyen Q De, Servis RL, Fung JM, Mylvaganam R, Mayr L, Gojo J, Haberler C, Geyeregger R, Czech T, Slavc I, Nahed B V., Curry WT, Carter BS, Wakimoto H, Brastianos PK, Batchelor TT, Stemmer-Rachamimov A, Martinez-Lage M, Frosch MP, Stamenkovic I, Riggi N, Rheinbay E, Monje M, Rozenblatt-Rosen O, Cahill DP, Patel AP, Hunter T, Verma IM, Ligon KL, Louis DN, Regev A, Bernstein BE, Tirosh I, Suvà ML. 2019. An Integrative Model of Cellular States, Plasticity, and Genetics for Glioblastoma. *Cell* 178:835-849.e21.

Nguyen-Chi M, Laplace-Builhe B, Travnickova J, Luz-Crawford P, Tejedor G, Phan QT, Duroux-Richard I, Levraud JP, Kissa K, Lutfalla G, Jorgensen C, Djouad F. 2015. Identification of polarized macrophage subsets in zebrafish. *Elife* 4:1–14.

Nimmerjahn A, Kirchhoff F, Helmchen F. 2005. Resting Microglial Cells Are Highly Dynamic Surveillants of Brain Parenchyma in Vivo. *Science* 308:1314–1318.
Ning S, Pagano JS, Barber GN. 2011. IRF7: Activation, regulation, modification and function. *Genes Immun* 12:399–414.

Ostrom QT, Gittleman H, Liao P, Vecchione-Koval T, Wolinsky Y, Kruchko C, Barnholtz-Sloan JS. 2017. CBTRUS Statistical Report: Primary brain and other central nervous system tumors diagnosed in the United States in 2010-2014. *Neuro Oncol* 19:v1–v88.
Park JH, Lee HK. 2022. Current Understanding of Hypoxia in Glioblastoma Multiforme and Its Response to Immunotherapy. *Cancers (Basel)* 14:1176.

Parmigiani E, Ivanek R, Rolando C, Hafen K, Turchinovich G, Lehmann FM, Gerber A, Brkic S, Frank S, Meyer SC, Wakimoto H, Günel M, Louvi A, Mariani L, Finke D, Holländer G, Hutter G, Tussiwand R, Taylor V, Giachino C. 2022. Interferon-γ resistance and immune evasion in glioma develop via Notch-regulated co-evolution of malignant and immune cells. *Dev Cell* 57:1847-1865.

Patel AP, Tirosh I, Trombetta JJ, Shalek AK, Gillespie SM, Wakimoto H, Cahill DP, Nahed B V., Curry WT, Martuza RL, Louis DN, Rozenblatt-Rosen O, Suvà ML, Regev A, Bernstein BE. 2014. Single-cell RNA-seq highlights intratumoral heterogeneity in primary glioblastoma. *Science (1979)* 344:1396–1401.

Pearson JRD, Cuzzubbo S, McArthur S, Durrant LG, Adhikaree J, Tinsley CJ, Pockley AG, McArdle. 2020. Immune Escape in Glioblastoma Multiforme and the Adaptation of Immunotherapies for Treatment. *Front Immunol* 15:582106.

Phillips HS, Kharbanda S, Chen R, Forrest WF, Soriano RH, Wu TD, Misra A, Nigro JM, Colman H, Soroceanu L, Williams PM, Modrusan Z, Feuerstein BG, Aldape K. 2006. Molecular subclasses of high-grade glioma predict prognosis, delineate a pattern of disease progression, and resemble stages in neurogenesis. *Cancer Cell* 9:157–173.
Pyonteck SM, Akkari L, Schuhmacher AJ, Bowman RL, Sevenich L, Quail DF, Olson OC, Quick ML, Huse JT, Teijeiro V, Setty M, Leslie CS, Oei Y, Pedraza A, Zhang J, Brennan CW, Sutton JC, Holland EC, Daniel D, Joyce JA. 2013. CSF-1R inhibition alters macrophage polarization and blocks glioma progression. *Nat Med* 19:1264–1272.

Quail DF, Joyce JA. 2017. The Microenvironmental Landscape of Brain Tumors. *Cancer Cell* 31:326-341.

Ren Jiangbin, Xu B, Ren Jianghao, Liu Z, Cai L, Zhang X, Wang W, Li S, Jin L, Ding L. 2023. The Importance of M1-and M2-Polarized Macrophages in Glioma and as Potential Treatment Targets. *Brain Sci* 13:1269.

Sengupta S, Marrinan J, Frishman C, Sampath P. 2012. Impact of temozolomide on immune response during malignant glioma chemotherapy. *Clin Dev Immunol* 2012:831090.

Shi ZF, Li GZ, Zhai Y, Pan CQ, Wang D, Yu MC, Liu C, Zhang W, Yu XG. 2023. EGFRvIII Promotes the Proneural–Mesenchymal Transition of Glioblastoma Multiforme and Reduces Its Sensitivity to Temozolomide by Regulating the NF-κB/ALDH1A3 Axis. *Genes (Basel)* 14:651.

Shiau CE, Kaufman Z, Meireles AM, Talbot WS. 2015. Differential requirement for irf8 in formation of embryonic and adult macrophages in zebrafish. *PLoS One* 10:1–15.
Shiau CE, Monk KR, Joo W, Talbot WS. 2013. An anti-inflammatory nod-like receptor is required for microglia development. *Cell Rep* 5:1342–1352.

Sichien D, Scott CL, Martens L, Vanderkerken M, Van Gassen S, Plantinga M, Joeris T, De Prijck S, Vanhoutte L, Vanheerswynghels M, Van Isterdael G, Toussaint W, Madeira FB, Vergote K, Agace WW, Clausen BE, Hammad H, Dalod M, Saeys Y, Lambrecht BN, Guilliams M. 2016. IRF8 Transcription Factor Controls Survival and Function of Terminally Differentiated Conventional and Plasmacytoid Dendritic Cells, Respectively. *Immunity* 45:626–640.

Smith ACH, Raimondi AR, Salthouse CD, Ignatius MS, Blackburn JS, Mizgirev I V., Storer NY, De Jong JLO, Chen AT, Zhou Y, Revskoy S, Zon LI, Langenau DM. 2010. High-throughput cell transplantation establishes that tumor-initiating cells are abundant in zebrafish T-cell acute lymphoblastic leukemia. *Blood* 115:3296–3303.
Subramanian A, Tamayo P, Mootha VK, Mukherjee S, Ebert BL, Gillette MA, Paulovich A, Pomeroy SL, Golub TR, Lander ES, Mesirov JP. 2005. Gene set enrichment analysis: A knowledge-based approach for interpreting genome-wide expression profiles. *Proc Natl Acad Sci* 102:15545-50.

Suwala AK, Stichel D, Schrimpf D, Maas SLN, Sill M, Dohmen H, Banan R, Reinhardt A, Sievers P, Hinz F, Blattner-Johnson M, Hartmann C, Schweizer L, Boldt HB, Kristensen BW,

Schittenhelm J, Wood MD, Chotard G, Bjergvig R, Das A, Tabori U, Hasselblatt M, Korshunov A, Abdullaev Z, Quezado M, Aldape K, Harter PN, Snuderl M, Hench J, Frank S, Acker T, Brandner S, Winkler F, Wesseling P, Pfister SM, Reuss DE, Wick W, von Deimling A, Jones DTW, Sahm F. 2021. Glioblastomas with primitive neuronal component harbor a distinct methylation and copy-number profile with inactivation of TP53, PTEN, and RB1. *Acta Neuropathol* 142:179–189.

Synthego. 2019. Synthego Performance Analysis, ICE Analysis.

Takke C, Dornseifer P, Weizsäcker E V., Campos-Ortega JA. 1999. her4, a zebrafish homologue of the Drosophila neurogenic gene E(spl), is a target of NOTCH signalling. *Development* 126:1811–1821.

Than-Trong E, Kiani B, Dray N, Ortica S, Simons B, Rulands S, Alunni A, Bally-Cuif L. 2020. Lineage hierarchies and stochasticity ensure the long-term maintenance of adult neural stem cells. *Sci Adv* 6:26–29.

Torp SH, Solheim O, Skjulsvik AJ. 2022. The WHO 2021 Classification of Central Nervous System tumours: a practical update on what neurosurgeons need to know—a minireview. *Acta Neurochir (Wien)* 164:2453–2464.

Verhaak RGW, Hoadley KA, Purdom E, Wang V, Qi Y, Wilkerson MD, Miller CR, Ding L, Golub T, Mesirov JP, Alexe G, Lawrence M, O'Kelly M, Tamayo P, Weir BA, Gabriel S, Winckler W, Gupta S, Jakkula L, Feiler HS, Hodgson JG, James CD, Sarkaria JN, Brennan C, Kahn A, Spellman PT, Wilson RK, Speed TP, Gray JW, Meyerson M, Getz G, Perou CM, Hayes DN. 2010. Integrated Genomic Analysis Identifies Clinically Relevant Subtypes of Glioblastoma Characterized by Abnormalities in PDGFRA, IDH1, EGFR, and NF1. *Cancer Cell* 17:98–110.

Wang Q, Hu B, Hu X, Kim H, Squatrito M, Scarpace L, deCarvalho AC, Lyu S, Li P, Li Y, Barthel F, Cho HJ, Lin YH, Satani N, Martinez-Ledesma E, Zheng S, Chang E, Sauvé CEG, Olar A, Lan ZD, Finocchiaro G, Phillips JJ, Berger MS, Gabrusiewicz KR, Wang G, Eskilsson E, Hu J, Mikkelsen T, DePinho RA, Muller F, Heimberger AB, Sulman EP, Nam DH, Verhaak RGW. 2017. Tumor Evolution of Glioma-Intrinsic Gene Expression Subtypes Associates with Immunological Changes in the Microenvironment. *Cancer Cell* 32:42-56.e6.

Wei Q, Clarke L, Scheidenhelm DK, Qian B, Tong A, Sabha N, Karim Z, Bock NA, Reti R, Swoboda R, Purev E, Lavoie JF, Bajenaru ML, Shannon P, Herlyn D, Kaplan D, Henkelman RM, Gutmann DH, Guha A. 2006. High-grade glioma formation results from postnatal Pten loss or mutant epidermal growth factor receptor expression in a transgenic mouse glioma model. *Cancer Res* 66:7429–7437.

Yan C, Brunson DC, Tang Q, Do D, Iftimia NA, Moore JC, Hayes MN, Welker AM, Garcia EG, Dubash TD, Hong X, Drapkin BJ, Myers DT, Phat S, Volorio A, Marvin DL, Ligorio M, Dershowitz L, McCarthy KM, Karabacak MN, Fletcher JA, Sgroi DC, Iafrate JA, Maheswaran S, Dyson NJ, Haber DA, Rawls JF, Langenau DM. 2019. Visualizing Engrafted Human Cancer and Therapy Responses in Immunodeficient Zebrafish. *Cell* 177:1903–1914.

Yang K, Shi Y, Luo M, Mao M, Zhang X, Chen C, Liu Y, He Z, Liu Q, Wang W, Luo C, Yin W, Wang C, Niu Q, Zeng H, Bian XW, Ping YF. 2022a. Identification of a unique tumor cell subset employing myeloid transcriptional circuits to create an immunomodulatory microenvironment in glioblastoma. *Oncoimmunology* 11:1–15.

Yang L, Rojas AM, Shiau CE. 2021. Liposomal clodronate-mediated macrophage depletion in the zebrafish model. *Bio Protoc* 11.

Yeo SY, Kim MJ, Kim HS, Huh TL, Chitnis AB. 2007. Fluorescent protein expression driven by her4 regulatory elements reveals the spatiotemporal pattern of Notch signaling in the nervous system of zebrafish embryos. *Dev Biol* 301:555–567.

Zhang Y, Dube C, Gibert M, Cruickshanks N, Wang B, Coughlan M, Yang Y, Setiady I, Deveau C, Saoud K, Grello C, Oxford M, Yuan F, Abounader R. 2018. The p53 pathway in glioblastoma. *Cancers (Basel)* 10:297.

Figure Legends

Figure 1. *her4.1*-driven over-expression of patient-relevant oncogenes drives glial-derived brain tumor formation in syngeneic *tp53* loss-of-function mutant zebrafish. (A) Schematic of modeling strategy where linearized transgene vectors with the zebrafish *her4.1* promoter driving human EGFR^{vIII}, human PI3KCA^{H1047R}, and mScarlet fluorescent protein are co-injected at the one-cell stage into syngeneic (CG1 strain) *tp53*$^{-/-}$ mutant zebrafish embryos. Starting at 15 days post fertilization (dpf), mosaic-injected zebrafish were screened for CNS tumor formation, indicated by mScarlet expression in the brain region of live zebrafish. Co-injection of *gfap:*GFP linearized transgene is used to assess glial-specific cell fate specification *in vivo*. **(B)** *her4.1:*mScarlet and *gfap:*GFP expression in the anterior CNS of mosaic-injected syngeneic (CG1 strain) *tp53*$^{-/-}$ zebrafish at 30dpf. **(C)** Whole brain dissected from a p53EPS mosaic-injected zebrafish at 30dpf. **(D)** Cumulative frequencies of mScarlet+ CNS lesions in syngeneic *tp53*$^{-/-}$ mutant (CG1*tp53*$^{-/-}$) and wild-type (CG1) zebrafish injected at the one cell stage with *her4.1:*EGFR^{vIII} (E), *her4.1:*PI3KCA^{H1047R} (P), and/or *her4.1:*mScarlet (S). **(E)** Syngeneic (CG1 strain) zebrafish at 30dpf engrafted with *her4.1:*mScarlet+/*gfap:*GFP+ brain tumor cells, following primary transplantation (1T) at 2dpf into the embryonic brain ventricle. **(F)** Whole brain dissected from engrafted syngeneic host (CG1) zebrafish at 30dpf. **(G)** FACS plot of bulk syngeneic host brain following primary transplant (1T) of *her4.1:*EGFR^{vIII} + *her4.1:*PI3KCA^{H1047R} + *her4.1:*mScarlet + *gfap:*GFP brain tumor cells. **(H-O)** Histological staining of uninjected control (H-K) and p53EPS tumor burdened brains (L-O). **(H,L)** Hematoxylin and eosin (H&E) staining of coronal sections highlighting telecephalon and diencephalon regions of representative control (H) and p53EPS (L) brains. **(I,M)** Proliferating Cell Nuclear Antigen (PCNA) staining of control (I) and p53EPS (M) brain sections. **(J,N)** Phosphorylated-ERK (p-

ERK) staining and quantifications reveal increased MAPK signaling pathway activation in p53EPS tumors ($p<0.001$, n=3 independent tumor sections). **(K,O)** Phosphorylated-Akt (p-Akt) staining and quantifications reveal increased Akt signaling pathway activity in p53EPS tumors ($p=0.007$, n=3 independent tumor sections). Scare bars represent 50μm.

Figure 2. RNA expression analysis establishes enrichment of mesenchymal glioblastoma and inflammation signatures in p53EPS model. (A) Principal component analysis (PCA) of mRNA sequencing from whole control injected brains (CTRL), p53EPS and p53KPS tumor-burdened brains. **(B)** Heatmap of normalized counts for genes upregulated in p53EPS tumor-burdened brains (log2FoldChange > 2, padj < 0.05), compared to whole control injected brains (CTRL). A selected list of upregulated transcripts is indicated. **(C)** Gene set enrichment analysis (GSEA) plots of published gene signatures for mesenchymal subtype glioblastoma for genes differentially regulated in p53EPS compared to control injected brains (McLendon et al., 2008; Wang et al., 2017). Normalized Enrichment Scores (NES) and nominal p-values are indicated. **(D)** Bar plot of Normalized Enrichment Scores from GSEA of Hallmark gene sets (Liberzon et al., 2011). **(E)** Volcano plots of differentially expressed genes between sorted mScarlet+ p53EPS tumor cells and control injected whole brain tissue (CTRL WB), as well as between sorted mScarlet-negative cells from p53EPS tumor-burdened brains and control injected whole brains (CTRL WB). **(F)** *her4.1:*mScarlet and *rag2:*EGFP expression in live zebrafish with a p53EPS tumor at 30 dpf. **(G)** FACS plot of p53EPS brain with *rag2*:EGFP co-expression from (F). **(H, I)** *her4.1:*mScarlet and *mpeg1.1:*EGFP expression in live zebrafish with a p53EPS tumor at 30 dpf.

Figure 3. p53EPS recruits activated microglia/macrophages at early stages of tumor initiation. (A-C) Neutral red staining of p53EPS mScarlet tumor-negative (A) and mScarlet tumor-positive brains (B,C) at 10 dpf. Neutral red foci in early-stage lesions are highlighted with arrows and are indicative of phagocytic cells. **(D)** Whole brain with p53EPS-induced tumor in a transgenic Tg(*tnfa:*EGFP) zebrafish at 20 dpf. **(E)** Z-stack projection of live confocal imaging of p53EPS tumor in transgenic Tg(*tnfa*:EGFP) background. **(F-K)** Z-stack projections of control uninjected (F-H) and p53EPS brains (I-K) at 5 dpf (F,I), 7 dpf (G,J), and 9 dpf (H,K) in transgenic Tg(*mpeg1.1*:EGFP) background. White arrows highlight an early-stage p53EPS lesion and associated *mpeg:*EGFP+ cells. **(L)** Z-stack projections of two independent p53EPS brains at 12 dpf in transgenic Tg(*mpeg1.1*:EGFP) background. **(M)** Quantification of tumor-associated *mpeg1.1*:EGFP+ cells with overlapping and/or internalized *her4.1:*mScarlet+ punctae (n=3 independent tumors).

Figure 4. Inflammation-associated *irf7* and *irf8* inhibit p53EPS formation *in vivo*. (A-C) Primary (1°) control (A), *irf7* CRISPR/Cas9 (B), and *irf8* CRISPR/Cas9 (C) injected p53EPS at 30 dpf. **(D)** p53EPS incidence at 30 dpf in control (n=3 independent experiments, 108 zebrafish), *irf7* CRISPR/Cas9 (***p<0.0001, Fisher's exact test, n=2 independent experiments, 31 zebrafish), and *irf8* CRISPR/Cas9 (*p=0.0155, Fisher's exact test, n= 2 independent experiments, 36 total injected zebrafish). **(E)** Representative fluorescent in situ hybridization (FISH) images of whole mount control p53EPG (**E**GFR^{vIII} + **P**I3KCA^{H1047} + **G**FP) and p53EPG + *irf7* CRISPR/Cas9-injected zebrafish at 8 dpf. p53EPG (GFP, magenta) and *irf7* (green) images represent Z-stack projections through tumor lesions (11 optical sections each). Merged images represent single optical sections at two spatially separated levels within control and *irf7* knock-down tumors. DAPI staining (blue) is used to label nuclei. White arrowheads highlight *irf7*

expression specific to the TME. Scale bars represent 10μm. **(F)** Tg(*her4.1*:Cas9-2A-EGFP) expression at 30 dpf. **(G)** mScarlet+ p53EPS at 30 dpf in Tg(*her4.1*:Cas9-2A-EGFP) injected with *irf7* gRNAs at the one-cell stage. **(H)** p53EPS incidence at 30 dpf in Tg(*her4.1*:Cas9-2A-EGFP)-negative gRNA-injected control siblings, and Tg(*her4.1*:Cas9-2A-EGFP) zebrafish injected at the one-cell stage with *irf7* or *irf8* gRNAs. n.s. not significant, Fisher's exact test.

Figure 5. Inflammation-associated phagocytes inhibit p53EPS tumor engraftment. (A,B) CG1 syngeneic host zebrafish at 20 dpf engrafted with p53EPS tumor cells transplanted with vehicle control (A) or Clodronate liposomes (B) at 2 dpf. **(C-E)** Quantification of p53EPS control engrafted and p53EPS tumors engrafted into CG1 host embryos with (C) Clodronate liposomes (p=0.0048, Fisher's exact test, n=2 independent experiments, total 56 transplanted vehicle control and 50 transplanted Clodrosome-injected hosts), (D) engrafted into *irf8* CRISPR/Cas9-injected into CG1 syngeneic host embryos (p=0.0002, Fisher's exact test, n=2 independent experiments, total 100 transplanted control and 74 transplanted *irf8* CRISPR/Cas9-injected hosts).

Figures

Figure 1

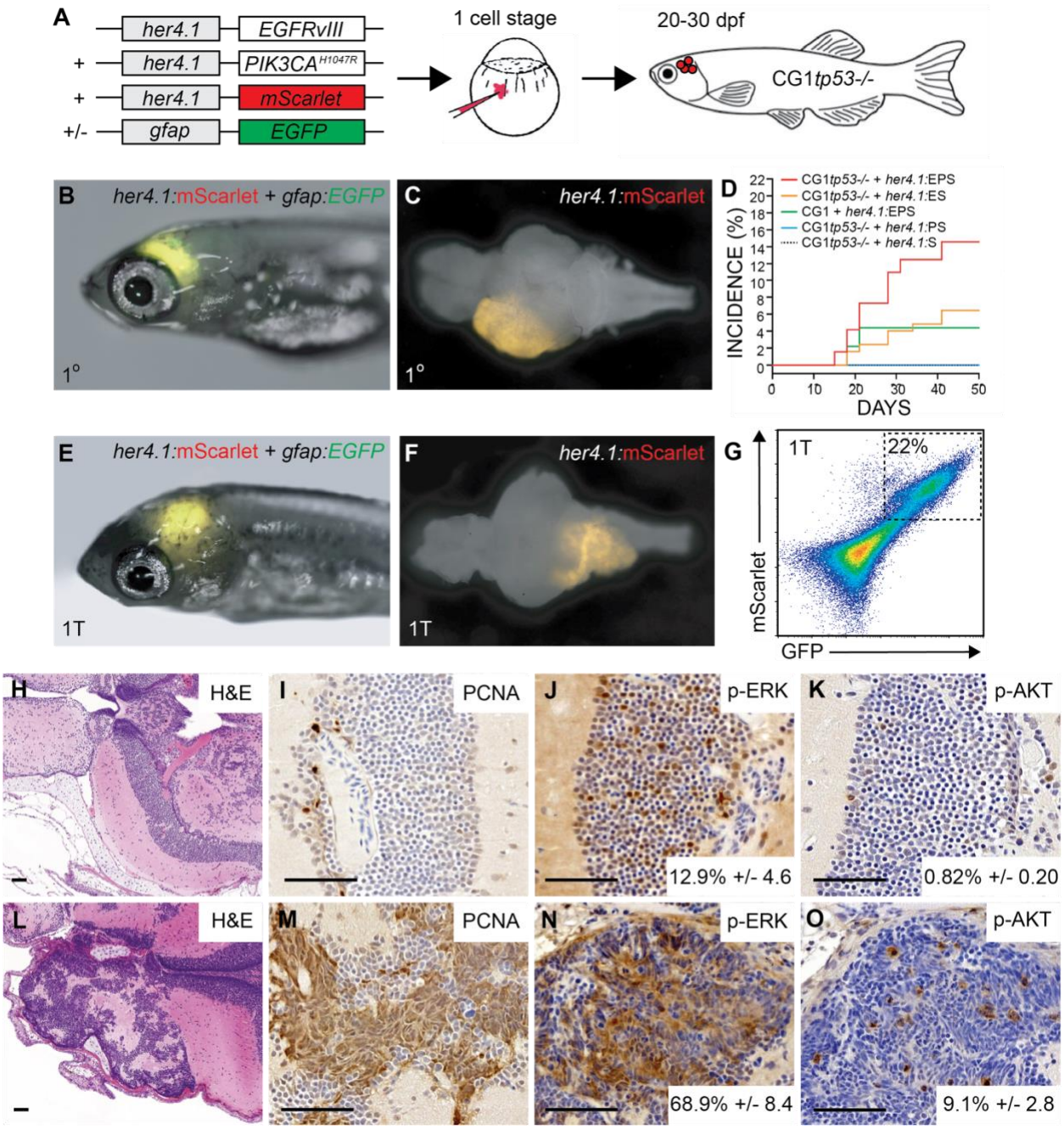

Figure 2

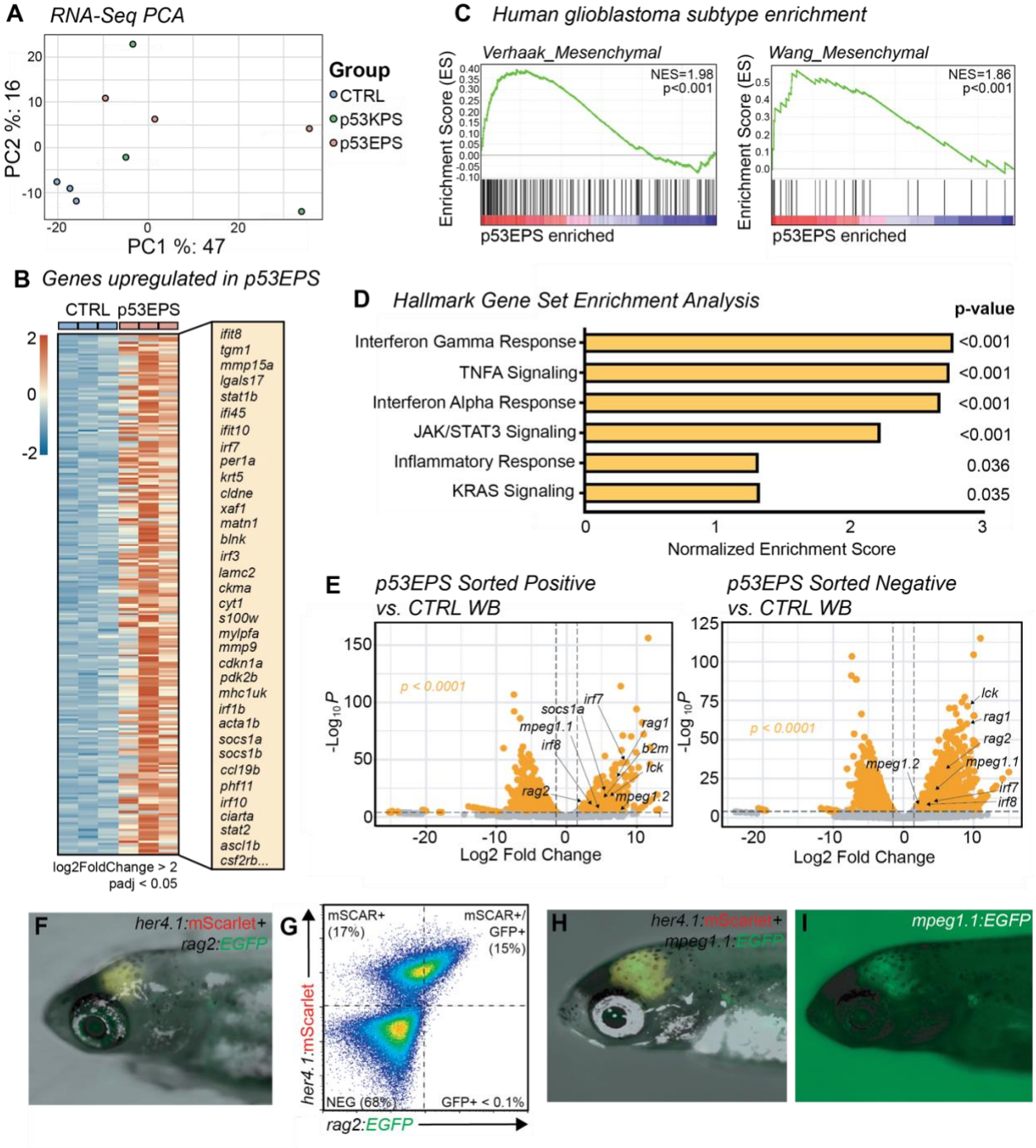
A RNA-Seq PCA
PC2 %: 16
PC1 %: 47
Group
CTRL
p53KPS
p53EPS
B Genes upregulated in p53EPS
CTRL p53EPS
ifit8
tgm1
mmp15a
lgals17
stat1b
ifi45
ifit10
irf7
per1a
krt5
cldne
xaf1
matn1
blnk
irf3
lamc2
ckma
cyt1
s100w
mylpfa
mmp9
cdkn1a
pdk2b
mhc1uk
irf1b
acta1b
socs1a
socs1b
ccl19b
phf11
irf10
ciarta
stat2
ascl1b
csf2rb...
log2FoldChange > 2
padj < 0.05
C Human glioblastoma subtype enrichment
Verhaak_Mesenchymal
NES=1.98
p<0.001
Wang_Mesenchymal
NES=1.86
p<0.001
Enrichment Score (ES)
p53EPS enriched
D Hallmark Gene Set Enrichment Analysis
p-value
Interferon Gamma Response <0.001
TNFA Signaling <0.001
Interferon Alpha Response <0.001
JAK/STAT3 Signaling <0.001
Inflammatory Response 0.036
KRAS Signaling 0.035
Normalized Enrichment Score
E p53EPS Sorted Positive vs. CTRL WB
p53EPS Sorted Negative vs. CTRL WB
p < 0.0001
socs1a
irf7
mpeg1.1
irf8
rag1
b2m
lck
rag2
mpeg1.2
-Log10P
Log2 Fold Change
F her4.1:mScarlet+ rag2:EGFP
G mSCAR+ (17%)
mSCAR+/ GFP+ (15%)
NEG (68%)
GFP+ < 0.1%
her4.1:mScarlet
rag2:EGFP
H her4.1:mScarlet+ mpeg1.1:EGFP
I mpeg1.1:EGFP

Figure 3

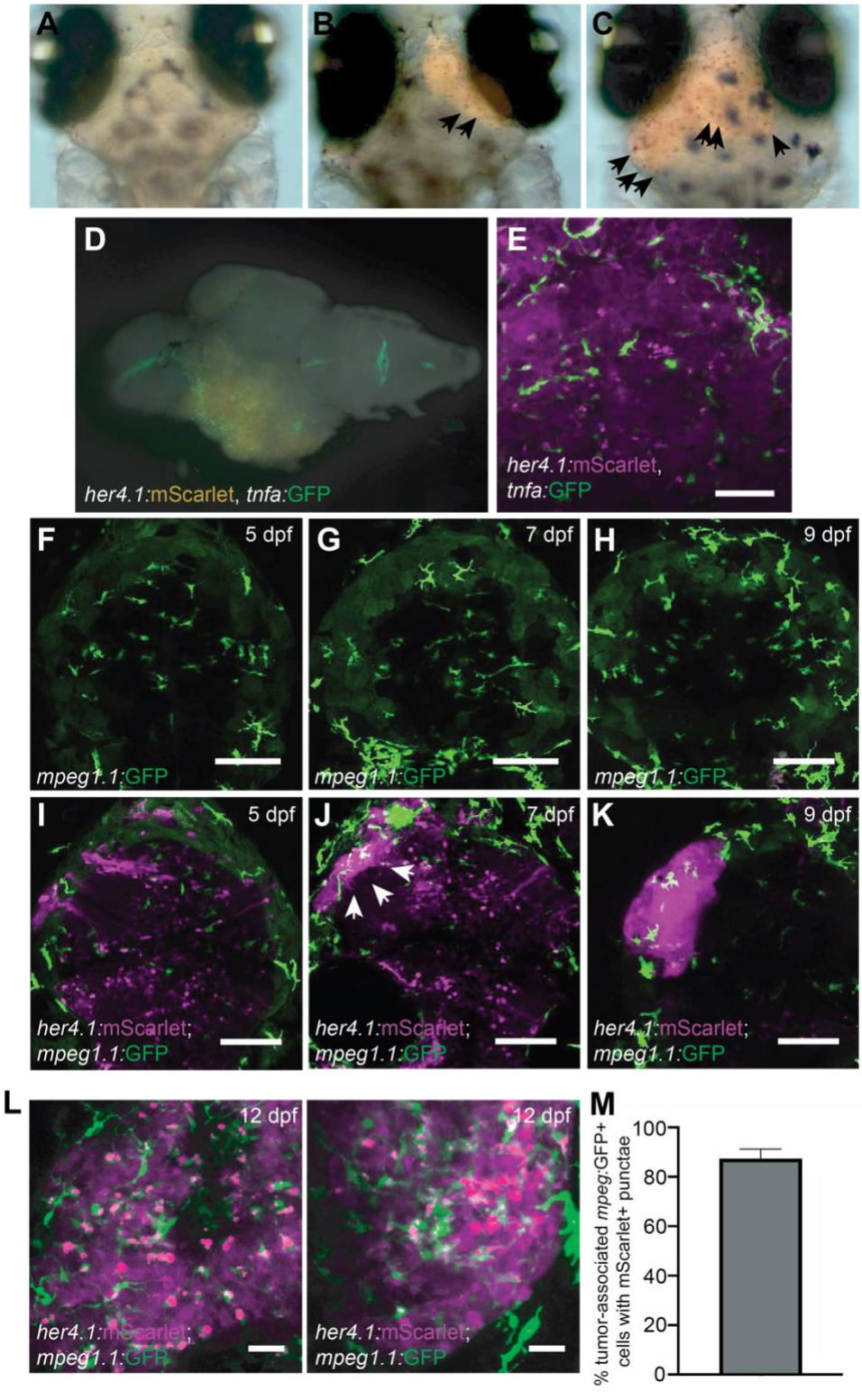
A
B
C
D
her4.1:mScarlet, tnfa:GFP
E
her4.1:mScarlet,
tnfa:GFP
F
5 dpf
mpeg1.1:GFP
G
7 dpf
mpeg1.1:GFP
H
9 dpf
mpeg1.1:GFP
I
5 dpf
her4.1:mScarlet;
mpeg1.1:GFP
J
7 dpf
her4.1:mScarlet;
mpeg1.1:GFP
K
9 dpf
her4.1:mScarlet;
mpeg1.1:GFP
L
12 dpf
her4.1:mScarlet;
mpeg1.1:GFP
12 dpf
her4.1:mScarlet;
mpeg1.1:GFP
M
% tumor-associated mpeg:GFP+
cells with mScarlet+ punctae
100
80
60
40
20
0

Figure 4

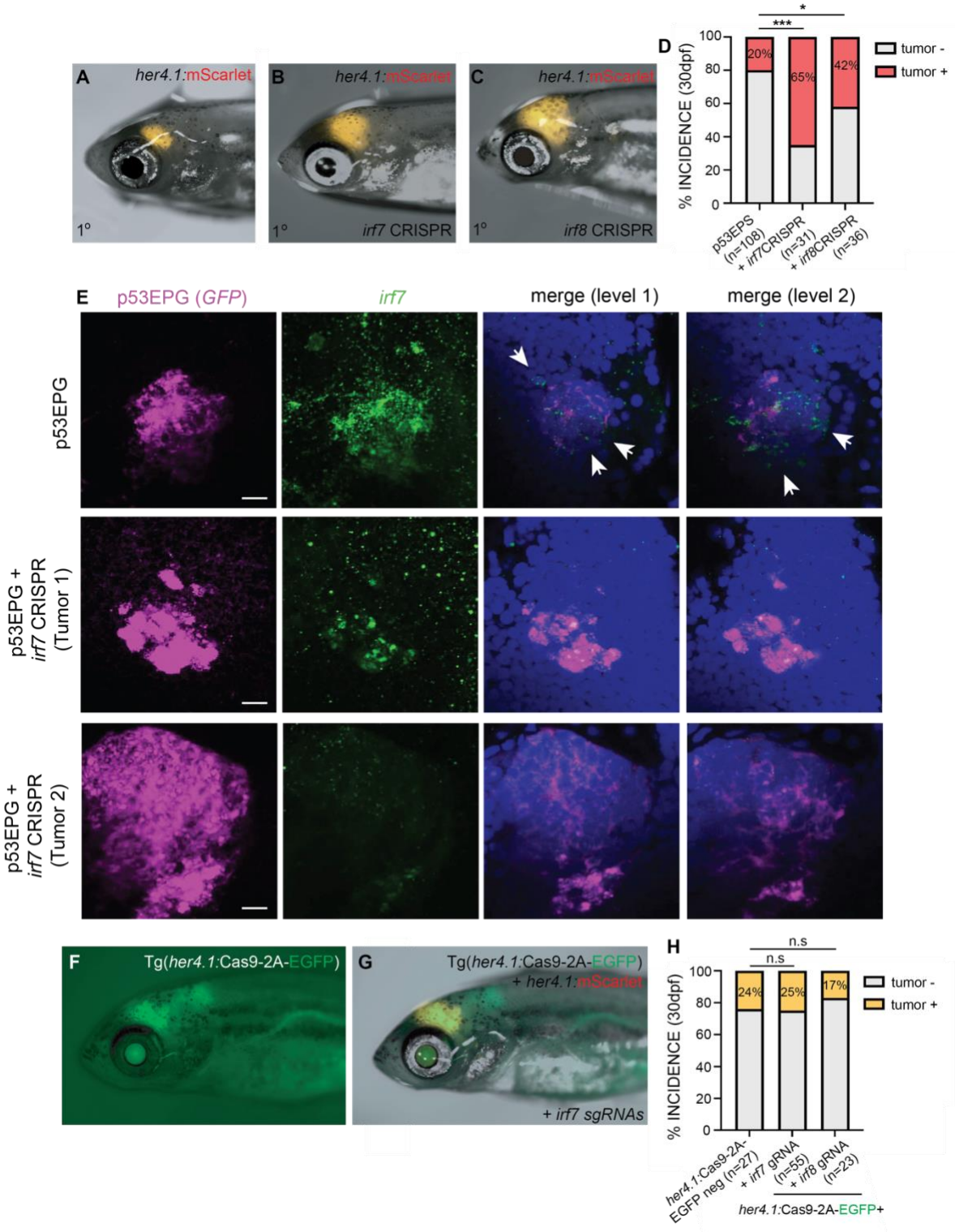
A
her4.1:mScarlet
1°
B
her4.1:mScarlet
1°
irf7 CRISPR
C
her4.1:mScarlet
1°
irf8 CRISPR
D
% INCIDENCE (30dpf)
100
80
60
40
20
0
20%
65%
42%
*
***
tumor -
tumor +
p53EPS (n=108)
+ irf7CRISPR (n=31)
+ irf8CRISPR (n=36)
E
p53EPG (GFP)
irf7
merge (level 1)
merge (level 2)
p53EPG
p53EPG + irf7 CRISPR (Tumor 1)
p53EPG + irf7 CRISPR (Tumor 2)
F
Tg(her4.1:Cas9-2A-EGFP)
G
Tg(her4.1:Cas9-2A-EGFP)
+ her4.1:mScarlet
+ irf7 sgRNAs
H
% INCIDENCE (30dpf)
100
80
60
40
20
0
24%
25%
17%
n.s
n.s
tumor -
tumor +
her4.1:Cas9-2A-EGFP neg (n=27)
+ irf7 gRNA (n=55)
+ irf8 gRNA (n=23)
her4.1:Cas9-2A-EGFP+

Figure 5

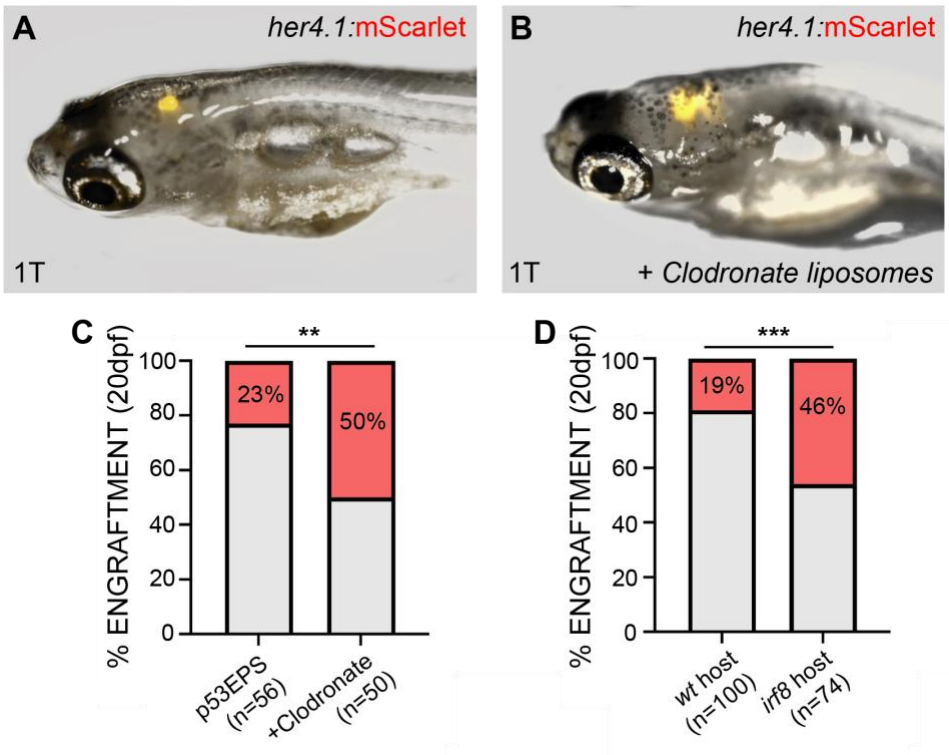
A
her4.1:mScarlet
1T
B
her4.1:mScarlet
1T
+ Clodronate liposomes
C
% ENGRAFTMENT (20dpf)
100
80
60
40
20
0
**
23%
50%
p53EPS (n=56)
+Clodronate (n=50)
D
% ENGRAFTMENT (20dpf)
100
80
60
40
20
0
***
19%
46%
wt host (n=100)
irf8 host (n=74)

Supplementary Figures

Supplementary Figure 1. Inter-tumoral heterogeneity in p53EPS induced tumors. Sample screens of p53EPS injected fish showing distinct tumor initiation sites and varying degrees of mScarlet-fluorescent intensity. Tumors predominantly arise in the optic tectum/mesencephalon region with a subset appearing in the telencephalon/diencephalon region. Distinct tumors did not arise in the cerebellum/rhombencephalon regions over the course of our experiments.

Supplementary Figure 2. Hematoxylin and eosin (H&E) staining of three independent p53EPS tumors. Scale bars represent 50μm.

Supplementary Figure 3. (A) *her4.1:*mScarlet and *gfap:*GFP expression in the anterior CNS of 30dpf syngeneic (CG1) *tp53*$^{-/-}$ zebrafish injected at the one-cell stage with linearized *her4.1:*KRAS^{G12D} + *her4.1:*PI3KCA^{H1047R} + *her4.1:*GFP + *gfap:*mScarlet transgenes. **(B)** Whole brain dissected from mosaic-injected *her4.1:*KRAS^{G12D} + *her4.1:*PI3KCA^{H1047R} + *her4.1:*GFP zebrafish at 30dpf. **(C)** Cumulative frequencies of GFP+ brain lesions in syngeneic *tp53*$^{-/-}$ mutant (CG1*tp53*$^{-/-}$) and wild-type (CG1) zebrafish injected at the one cell stage with *her4.1:*KRAS^{G12D} (K), *her4.1:*PI3KCA^{H1047R} (P), and/or *her4.1:*GFP (G). **(D)** Immunohistochemical staining of proliferating cell nuclear antigen (PCNA), phosphorylated ERK (p-ERK), and phosphorylated AKT (p-AKT) on *her4.1:*KRAS^{G12D} + *her4.1:*PI3KCA^{H1047R} + *her4.1:*GFP tumor section. Quantification of p-ERK and p-AKT positive cells within total field. Scale bars represent 50μm.

Supplementary Figure 4. Gene set enrichment analysis (GSEA) plots of published gene signatures for alternative molecular subtypes of human glioblastoma and medulloblastoma for

genes differentially regulated in p53EPS compared to control injected brains (Cavalli et al., 2017; McLendon et al., 2008; Wang et al., 2017). Normalized Enrichment Scores (NES) and nominal p-values are indicated.

Supplementary Figure 5. Quantitative real-time PCR analysis of neural stem cell (NSC) genes and genes associated with inflammatory gene expression signatures identified using bulk RNA sequencing. Gene expression in pooled *her4.1:*mScarlet+/*gfap:*GFP+ FACS-sorted cells relative to non-tumor control brain tissue. *p<0.01, **p<0.001, Student's t-test.

Supplementary Figure 6. Gene set enrichment analysis (GSEA) plots of established gene signatures for classical M1 polarized macrophages (Classical_M1_VS_Alternative_M2_Macrophage_UP), compared to alternative M2 macrophages (Classical_M1_VS_Alternative_M2_Macrophage_DN). GSEA plots of macrophage-specific gene expression at early (DAY3 UP) and late (DAY3 Down) time points of stimulation with macrophage colony stimulating factor (MCSF). Normalized Enrichment Scores (NES) and nominal p-values are indicated.

Supplementary Figure 7. Quantitative real-time PCR analysis of *irf7* CRISPR/Cas9-injected **(A)** and *irf8* CRISPR/Cas9-injected p53EPS **(B)**. Gene expression is represented relative to control p53EPS tumor-burdened whole brains. At least 5 tumor-burdened brains were pooled for each cohort and expression was normalized to mScarlet mRNA expression to account for differences in tumor size. *p<0.01, Student's t-test.

Supplementary Figure 8. (A,B) Images of neutral red staining in control (A) and *irf8* CRISPR/Cas9-injected (B) zebrafish larvae at 8 dpf, A' and B' highlight boxed regions. Black arrows highlight examples of neutral red foci. **(C)** Quantification of neutral red foci. *p<0.01, n=4 fish for each cohort, Student's t-test.

Supplementary Figure 9. (A) Quantitative real-time PCR analysis of neural stem cell (NSC) genes and inflammation genes in non-tumor control brains, pooled p53EPS-burdened brains and pooled brains engrafted with p53EPS tumor cells at 20 dpf. *p<0.01 compared to non-tumor control whole brain tissue, Student's t-test. **(B)** Quantitative real-time PCR analysis of neural stem cell (NSC) genes and inflammation genes at 20 dpf in primary transplanted (1T) p53EPS-burdened brains injected with vehicle control liposomes (1T p53EPS) and Clodrosomes at 2 dpf. At least 5 tumor-burdened brains were pooled for each cohort and expression was normalized to mScarlet mRNA expression to account for differences in tumor size. *p<0.01 compared to 1T p53EPS, Student's t-test.

Supplementary Movie 1. Time-lapse confocal images of p53EPS brain at 12 dpf in transgenic Tg(*mpeg1.1*:EGFP) background.

Supplementary Movie 2. Time-lapse confocal images of individual *her4.1:*mScarlet+ p53EPS and *mpeg1.1:*EGFP+ cells at 12 dpf.

Supplementary Figure 1

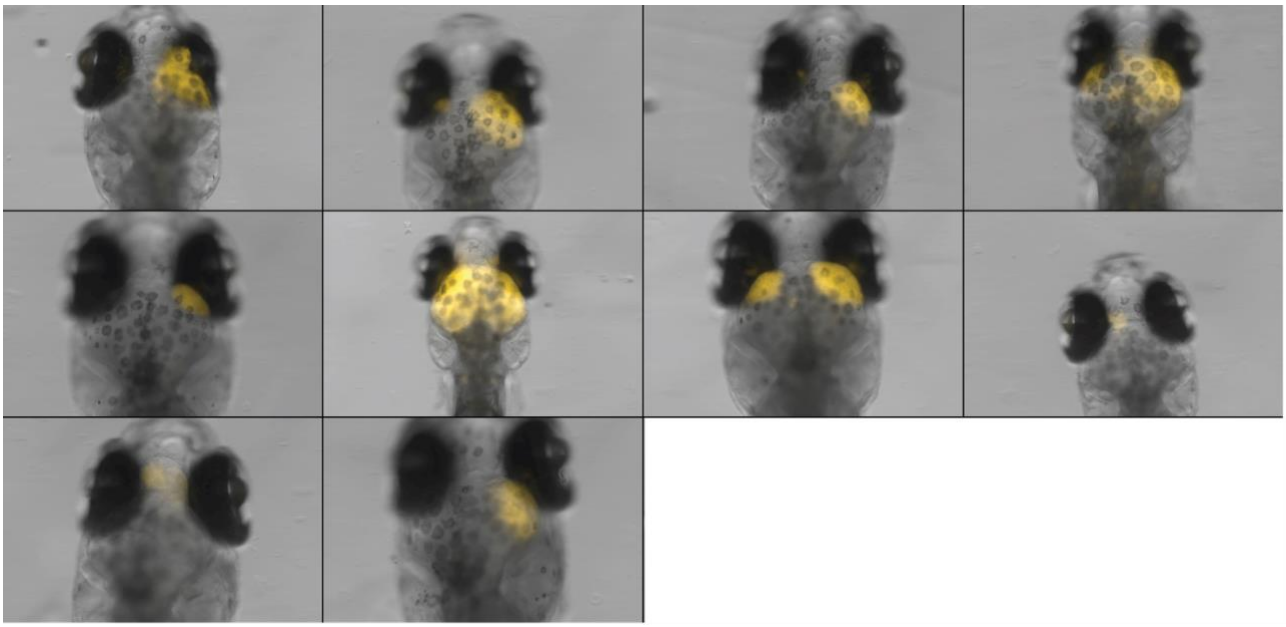

Supplementary Figure 2

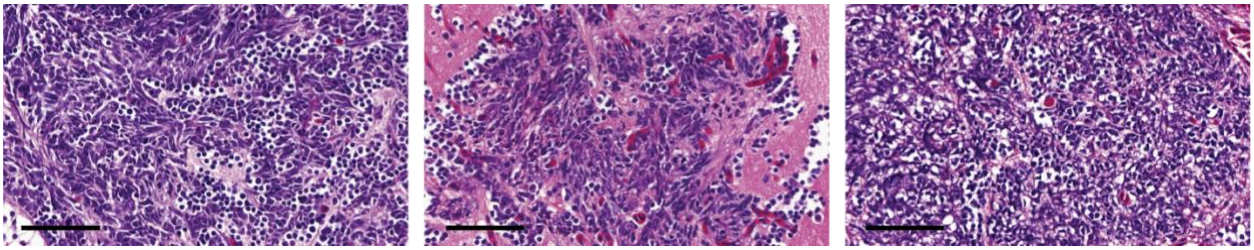

Supplementary Figure 3

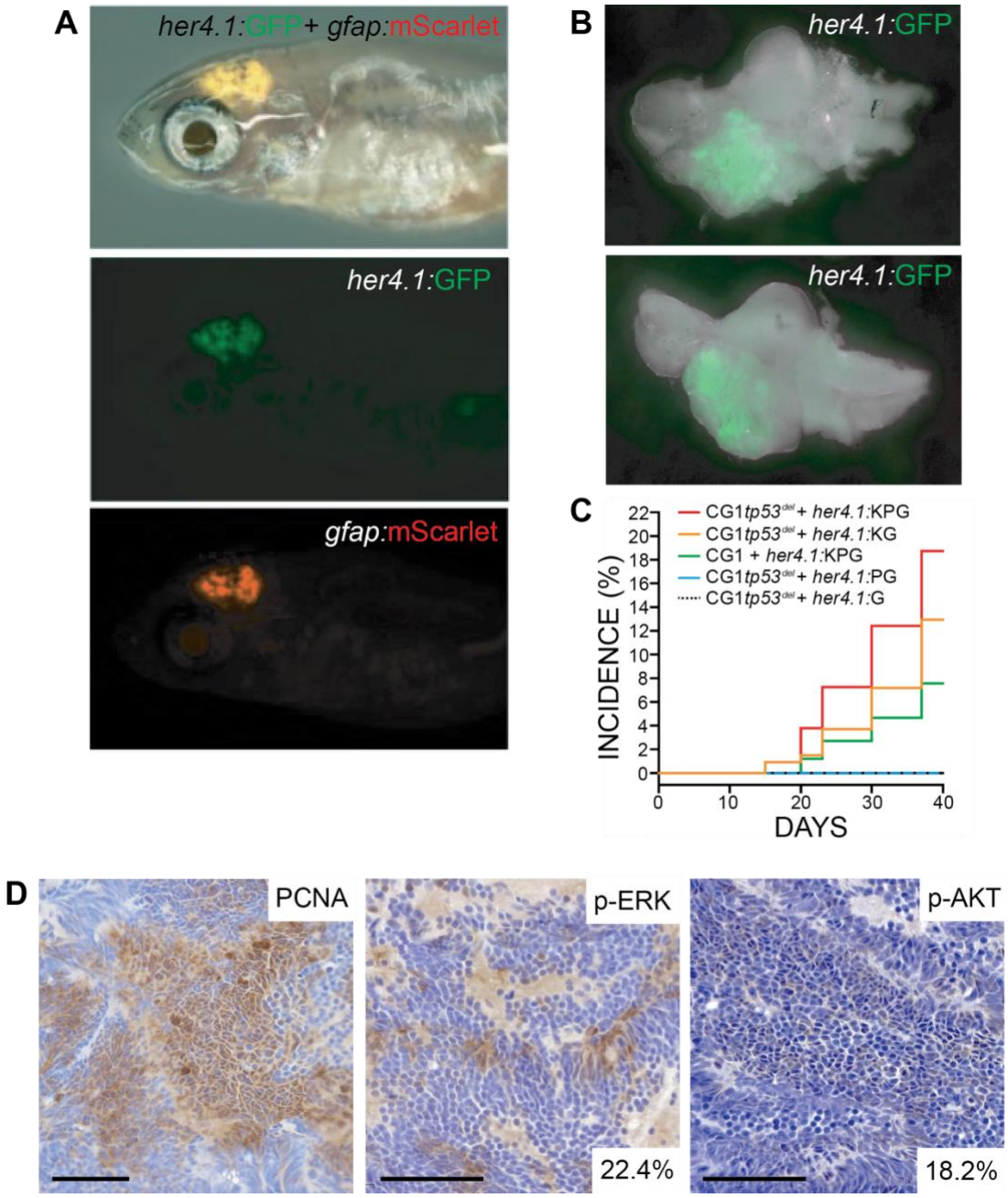

Supplementary Figure 4

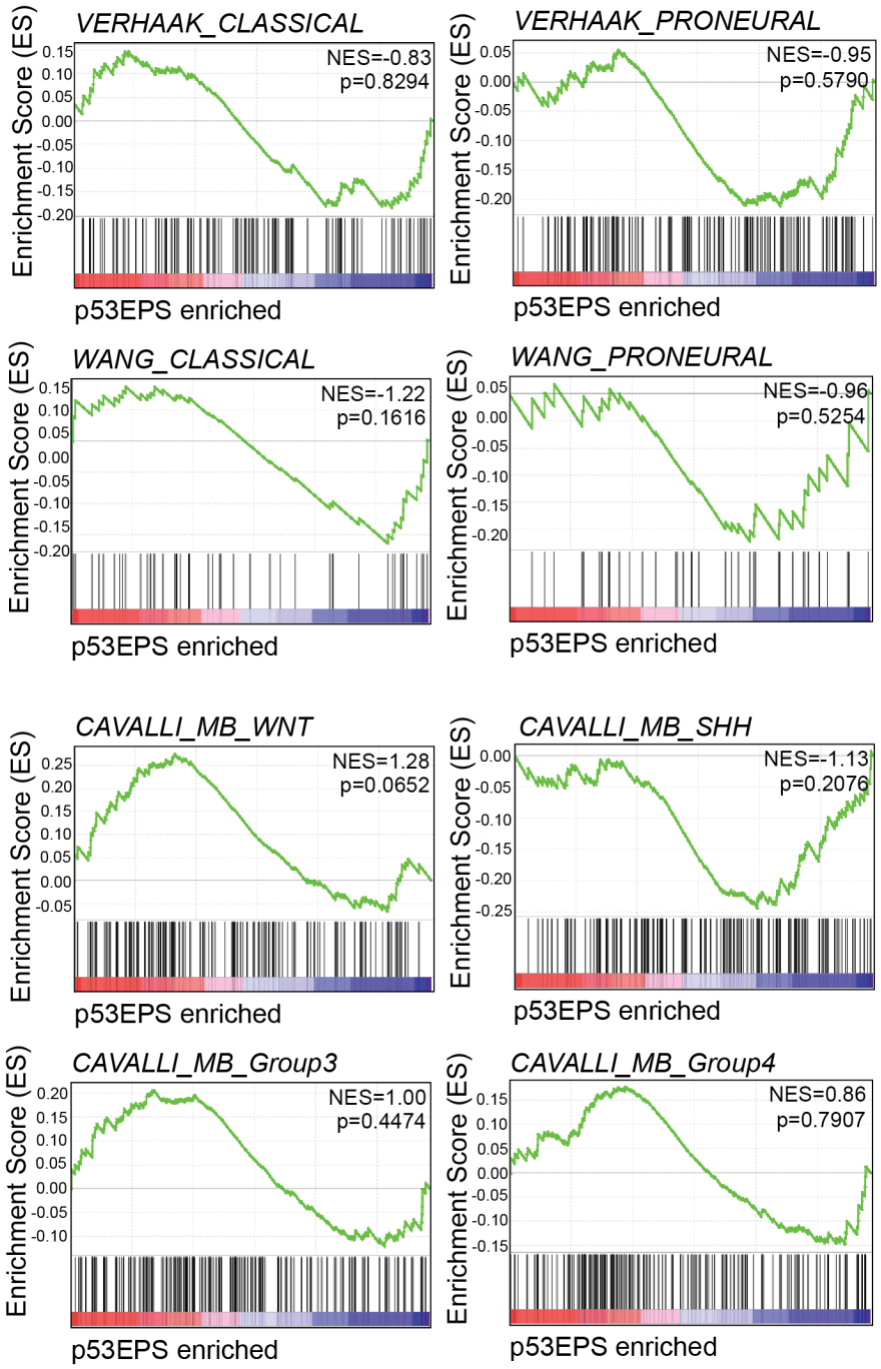

Supplementary Figure 5

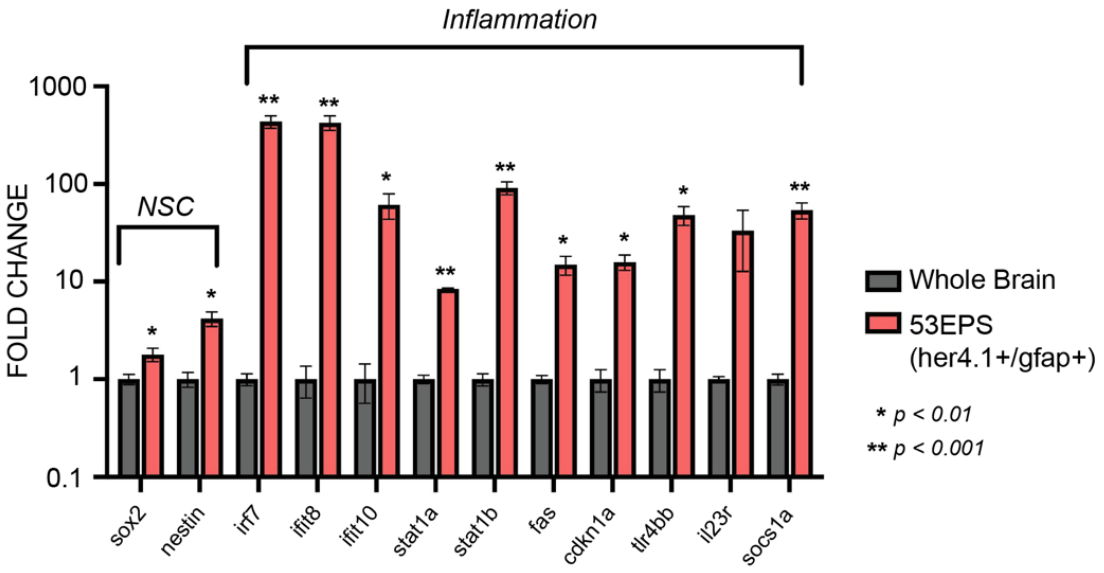

Supplementary Figure 6

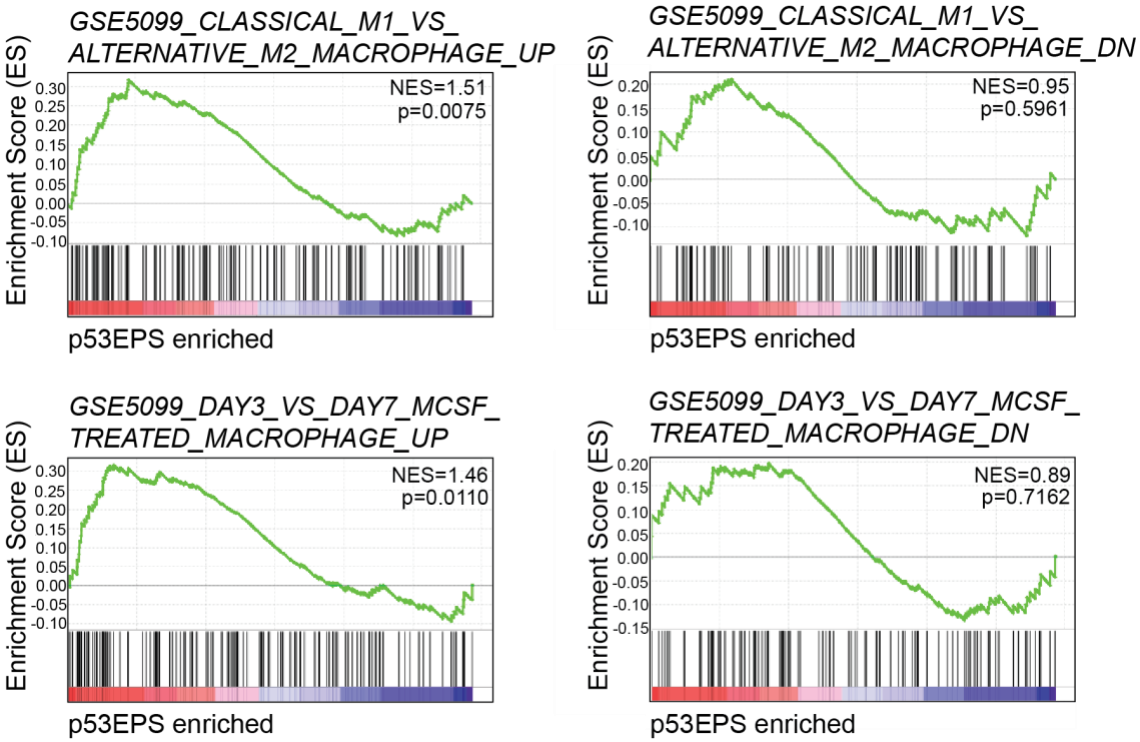

Supplementary Figure 7

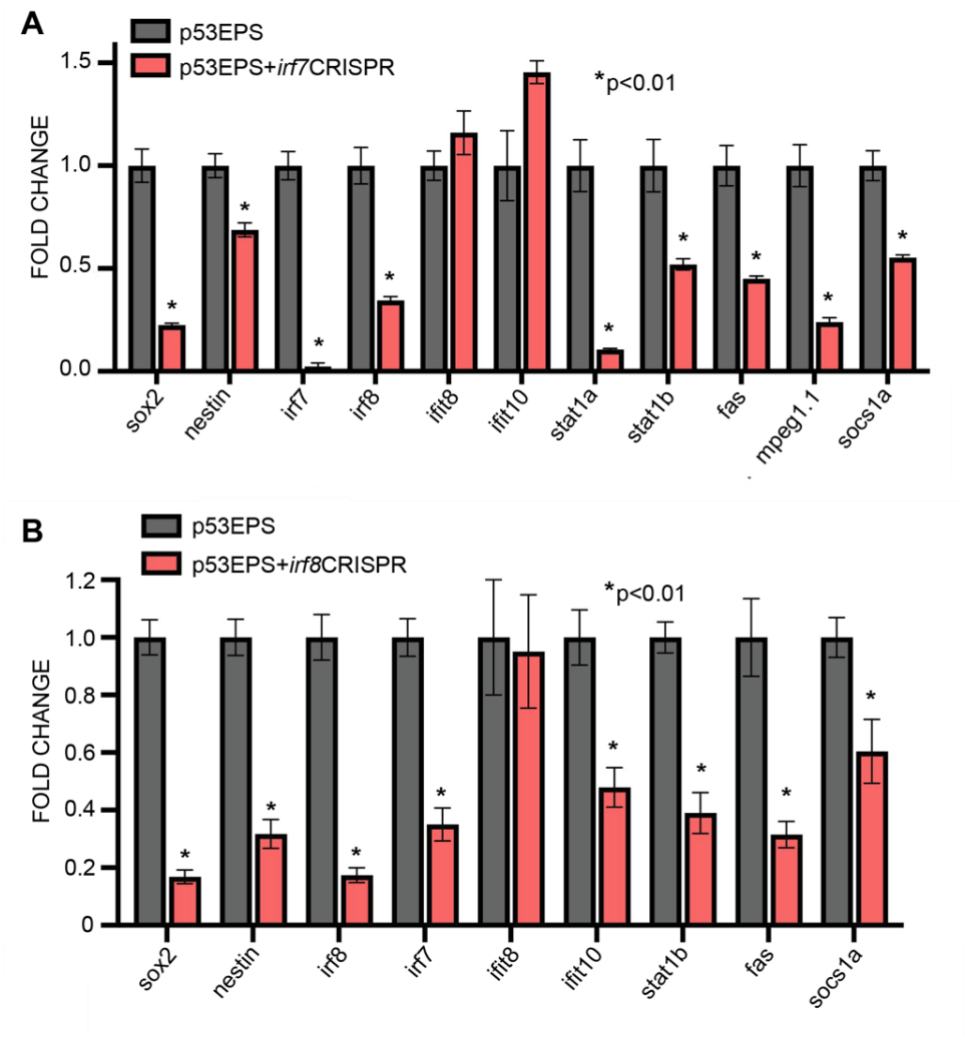

Supplementary Figure 8

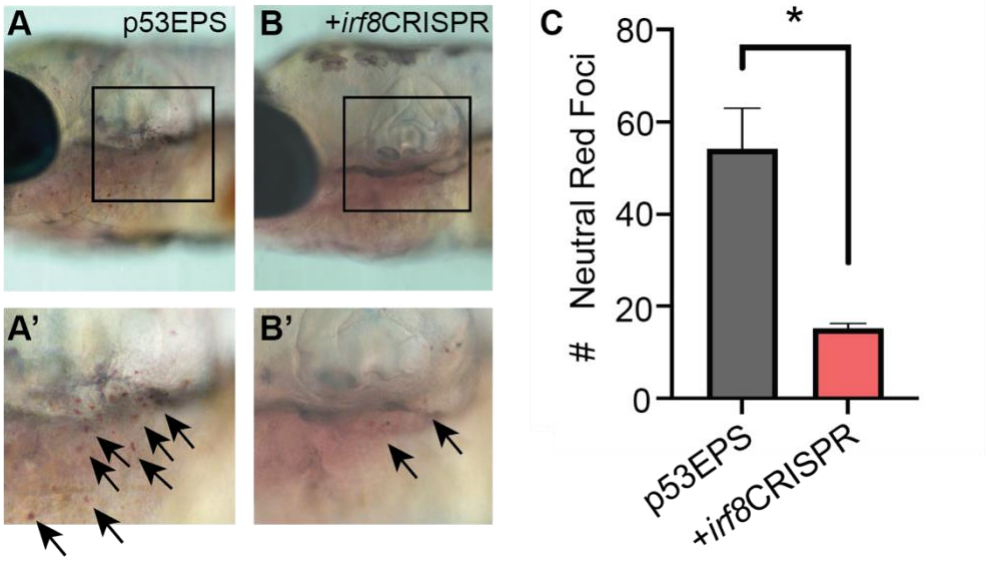
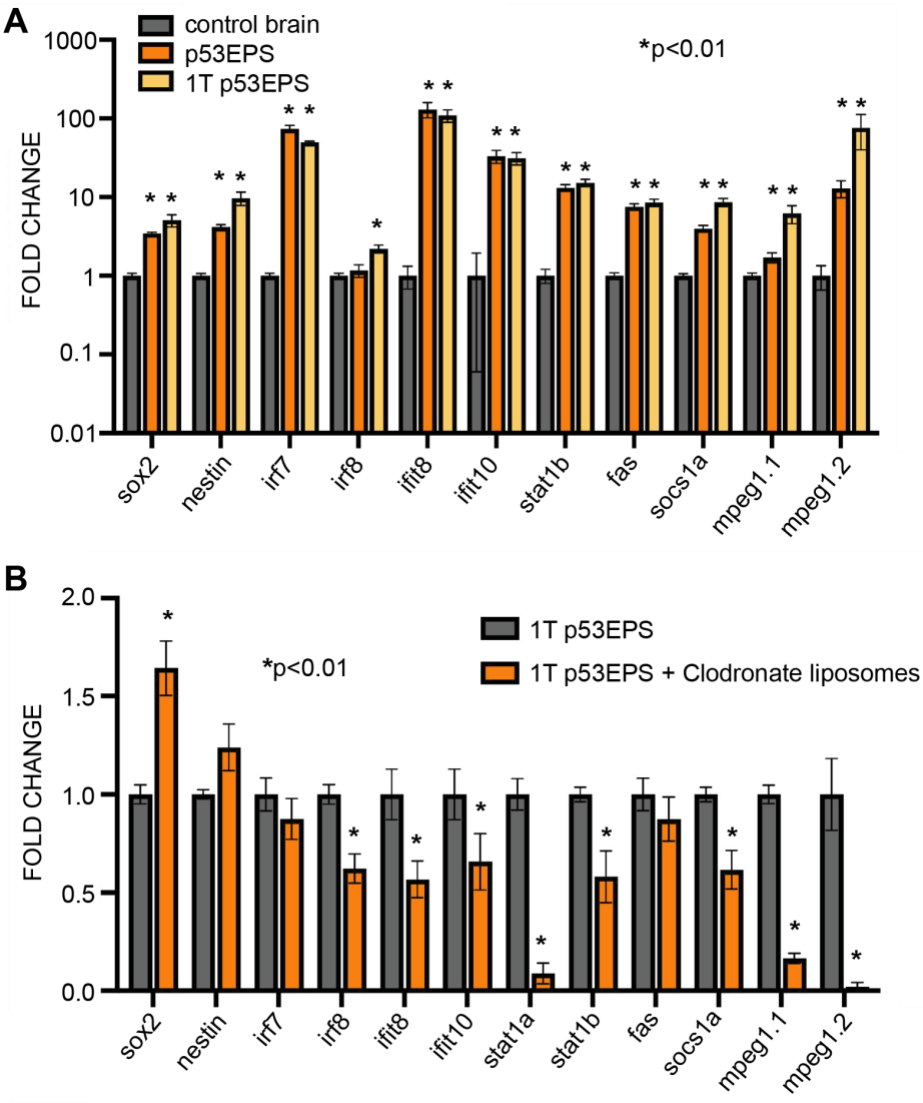
Supplementary Figure 9